

---

# PFDiff: Training-free Acceleration of Diffusion Models through the Gradient Guidance of Past and Future

---

Guangyi Wang<sup>1</sup>, Yuren Cai<sup>1</sup>, Lijiang Li<sup>1</sup>, Wei Peng<sup>2</sup>, Songzhi Su<sup>1\*</sup>

<sup>1</sup>School of Informatics, Xiamen University

<sup>2</sup>Department of Psychiatry and Behavioral Sciences, Stanford University

{wangguangyi, caiyuren, lilijiang}@stu.xmu.edu.cn,

wepeng@stanford.edu, ssz@xmu.edu.cn

## Abstract

Diffusion Probabilistic Models (DPMs) have shown remarkable potential in image generation, but their sampling efficiency is hindered by the need for numerous denoising steps. Most existing solutions accelerate the sampling process by proposing fast ODE solvers. However, the inevitable discretization errors of the ODE solvers are significantly magnified when the number of function evaluations (NFE) is fewer. In this work, we propose *PFDiff*, a novel *training-free* and *orthogonal* timestep-skipping strategy, which enables existing fast ODE solvers to operate with fewer NFE. Specifically, PFDiff initially utilizes gradient replacement from past time steps to predict a “springboard”. Subsequently, it employs this “springboard” along with foresight updates inspired by Nesterov momentum to rapidly update current intermediate states. This approach effectively reduces unnecessary NFE while correcting for discretization errors inherent in first-order ODE solvers. Experimental results demonstrate that PFDiff exhibits flexible applicability across various pre-trained DPMs, particularly excelling in conditional DPMs and surpassing previous state-of-the-art training-free methods. For instance, using DDIM as a baseline, we achieved 16.46 FID (4 NFE) compared to 138.81 FID with DDIM on ImageNet 64x64 with classifier guidance, and 13.06 FID (10 NFE) on Stable Diffusion with 7.5 guidance scale.

## 1 Introduction

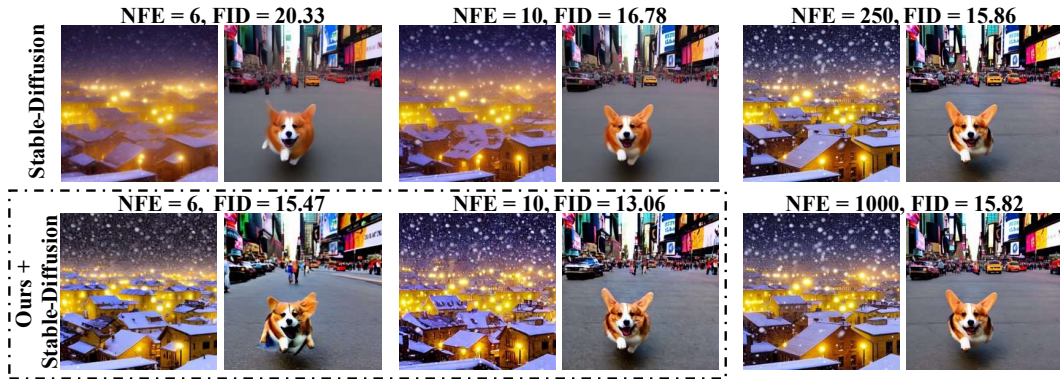
In recent years, Diffusion Probabilistic Models (DPMs) [1–4] have demonstrated exceptional modeling capabilities across various domains including image generation [5–7], video generation [8], text-to-image generation [9, 10], speech synthesis [11], and text-to-3D generation [12, 13]. They have become a key driving force advancing deep generative models. DPMs initiate with a forward process that introduces noise onto images, followed by utilizing a neural network to learn a backward process that incrementally removes noise, thereby generating images [2, 4]. Compared to other generative methods such as Generative Adversarial Networks (GANs) [14] and Variational Autoencoders (VAEs) [15], DPMs not only possess a simpler optimization target but also are capable of producing higher quality samples [5]. However, the generation of high-quality samples via DPMs requires hundreds or thousands of denoising steps, significantly lowering their sampling efficiency and becoming a major barrier to their widespread application.

Existing techniques for rapid sampling in DPMs primarily fall into two categories. First, training-based methods [16–19], which can significantly compress sampling steps, even achieving single-

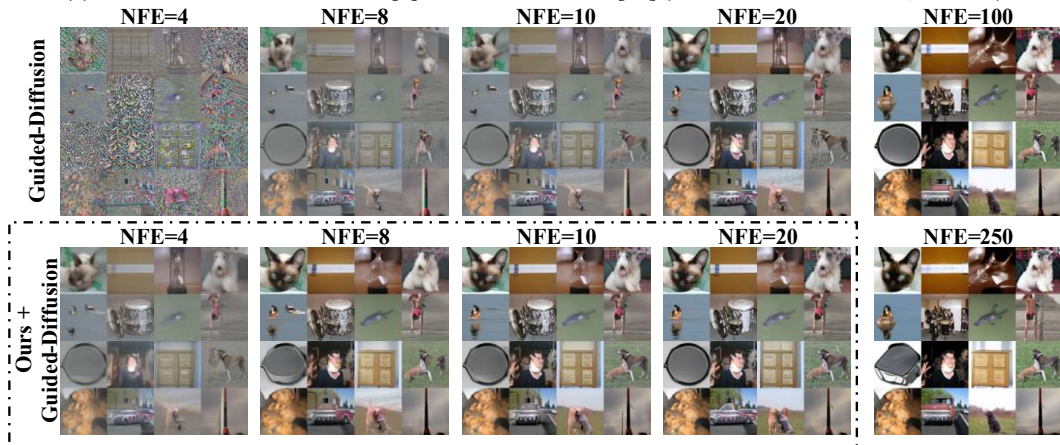
---

\*Corresponding Author.

Text Prompts: Winter night with snow -covered rooftops and soft yellow lights. (Left)  
 A Corgi running towards me in Times Square. (Right)



(a) Results from Stable-Diffusion [9] on MS-COCO2014 [32] (Classifier-Free Guidance,  $s = 7.5$ )



(b) Results from Guided-Diffusion [5] on ImageNet 64x64 [33] (Classifier Guidance,  $s = 1.0$ )

Figure 1: Sampling by conditional pre-trained DPMs [5, 9] using DDIM [20] and our method PFDiff (dashed box) with DDIM as a baseline, varying the number of function evaluations (NFE).

step sampling [19]. However, this compression often comes with a considerable additional training cost, and these methods are challenging to apply to large pre-trained models. Second, training-free samplers [20–31], which typically employ implicit or analytical solutions to Stochastic Differential Equations (SDE)/Ordinary Differential Equations (ODE) for lower-error sampling processes. For instance, Lu et al. [21, 22], by analyzing the semi-linear structure of the ODE solvers for DPMs, have sought to analytically derive optimally the solutions for DPMs’ ODE solvers. These training-free sampling strategies can often be used in a plug-and-play fashion, compatible with existing pre-trained DPMs. However, when the NFE is below 10, the discretization error of these training-free methods will be significantly amplified, leading to convergence issues [21, 22], which can still be time-consuming.

To further enhance the sampling speed of DPMs, we have analyzed the potential for improvement in existing training-free accelerated methods. Initially, we observed a high similarity in the model’s outputs for the existing ODE solvers when time step size  $\Delta t$  is not extremely large, as illustrated in Fig. 2a. This observation led us to utilize the gradients that have been computed from past time steps to approximate current gradients, thereby predicting a “springboard”. Furthermore, due to the similarities between the sampling process of DPMs and Stochastic Gradient Descent (SGD) [34] as noted in Remark 1, we incorporated a *foresight* update mechanism using Nesterov momentum [35], known for accelerating SGD training. Specifically, we first predict future gradients using the “springboard” to reduce errors, as shown in Fig. 2b. Then, we further replace the current gradients with the future gradients to facilitate a larger update step size  $\Delta t$ , as shown in Fig. 2c.

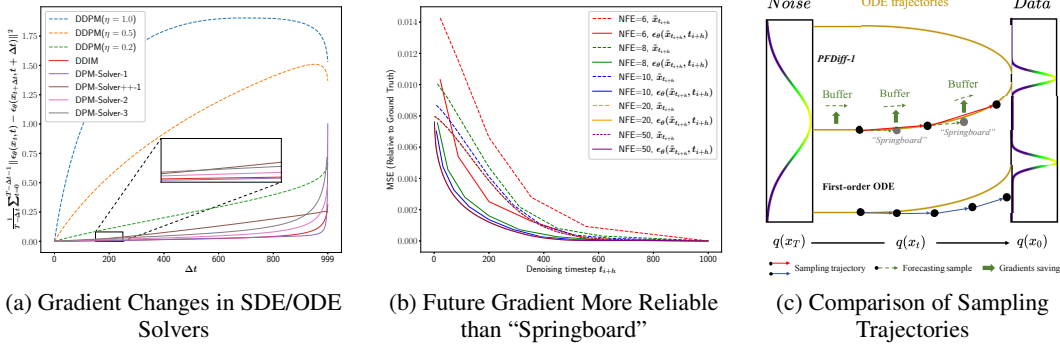


Figure 2: (a) The trend of the MSE of the noise network output  $\epsilon_\theta(x_t, t)$  over time step size  $\Delta t$ , where  $\eta$  comes from  $\bar{\sigma}_t$  in Eq. (6). Solid lines: ODE solvers, dashed lines: SDE solvers. (b) MSE relative to *ground truth* from sampling of 1000 NFE: “Springboard”  $\|\tilde{x}_{t_{i+h}} - \tilde{x}_{t_{i+h}}^{gt}\|^2$ ; Future Gradient  $\|\epsilon_\theta(\tilde{x}_{t_{i+h}}, t_{i+h}) - \epsilon_\theta(\tilde{x}_{t_{i+h}}^{gt}, t_{i+h})\|^2$ . (c) Comparison of partial sampling trajectories between PFDiff-1 and a first-order ODE solver, where the update directions are guided by the tangent direction of the sampling trajectories.

Motivated by these insights, we propose *PFDiff*, a timestep-skipping sampling algorithm that rapidly updates the current intermediate state through the gradient guidance of past and future. Notably, *PFDiff* is *training-free* and *orthogonal* to existing DPMs sampling algorithms, providing a new orthogonal axis for DPMs sampling. Furthermore, we prove that *PFDiff*, despite utilizing fewer NFE, corrects for errors in the sampling trajectories of first-order ODE solvers, as visualized in Fig. 2c. This ensures that improving sampling speed does not compromise sampling quality; it only reduces unnecessary NFE in existing ODE solvers. To validate the orthogonality and effectiveness of *PFDiff*, extensive experiments were conducted on both unconditional [2, 4, 20] and conditional [5, 9] pre-trained DPMs, with the visualization experiment of conditional DPMs depicted in Fig. 1. The results indicate that *PFDiff* significantly enhances the sampling performance of existing ODE solvers. Particularly in conditional DPMs, *PFDiff*, using only DDIM as the baseline, surpasses the previous state-of-the-art training-free sampling algorithms.

## 2 Background

### 2.1 Diffusion SDEs

Diffusion Probabilistic Models (DPMs) [1–4] aim to generate  $D$ -dimensional random variables  $x_0 \in \mathbb{R}^D$  that follow a data distribution  $q(x_0)$ . Taking Denoising Diffusion Probabilistic Models (DDPM) [2] as an example, these models introduce noise to the data distribution through a forward process defined over discrete time steps, gradually transforming it into a standard Gaussian distribution  $x_T \sim \mathcal{N}(\mathbf{0}, \mathbf{I})$ . The forward process’s latent variables  $\{x_t\}_{t \in [0, T]}$  are defined as follows:

$$q(x_t | x_0) = \mathcal{N}(x_t | \alpha_t x_0, \sigma_t^2 \mathbf{I}), \quad (1)$$

where  $\alpha_t$  is a scalar function related to the time step  $t$ , with  $\alpha_t^2 + \sigma_t^2 = 1$ . In the model’s reverse process, DDPM utilizes a neural network model  $p_\theta(x_{t-1} | x_t)$  to approximate the transition probability  $q(x_{t-1} | x_t, x_0)$ ,

$$p_\theta(x_{t-1} | x_t) = \mathcal{N}(x_{t-1} | \mu_\theta(x_t, t), \sigma_\theta^2(t) \mathbf{I}), \quad (2)$$

where  $\sigma_\theta^2(t)$  is defined as a scalar function related to the time step  $t$ . By sampling from a standard Gaussian distribution and utilizing the trained neural network, samples following the data distribution  $p_\theta(x_0) = \prod_{t=1}^T p_\theta(x_{t-1} | x_t)$  can be generated.

Furthermore, Song et al. [4] introduced SDE to model DPMs over continuous time steps, where the forward process is defined as:

$$dx_t = f(t)x_t dt + g(t)dw_t, \quad x_0 \sim q(x_0), \quad (3)$$

where  $w_t$  represents a standard Wiener process, and  $f$  and  $g$  are scalar functions of the time step  $t$ . It’s noteworthy that the forward process in Eq. (1) is a discrete form of Eq. (3), where  $f(t) = \frac{d \log \alpha_t}{dt}$

and  $g^2(t) = \frac{d\sigma_t^2}{dt} - 2\frac{d\log\alpha_t}{dt}\sigma_t^2$ . Song et al. [4] further demonstrated that there exists an equivalent reverse process from time step  $T$  to 0 for the forward process in Eq. (3):

$$dx_t = [f(t)x_t - g^2(t)\nabla_x \log q_t(x_t)] dt + g(t)d\bar{w}_t, \quad x_T \sim q(x_T), \quad (4)$$

where  $\bar{w}$  denotes a standard Wiener process. In this reverse process, the only unknown is the *score function*  $\nabla_x \log q_t(x_t)$ , which can be approximated through neural networks.

## 2.2 Diffusion ODEs

In DPMs based on SDE, the discretization of the sampling process often requires a significant number of time steps to converge, such as the  $T = 1000$  time steps used in DDPM [2]. This requirement primarily stems from the randomness introduced at each time step by the SDE. To achieve a more efficient sampling process, Song et al. [4] utilized the Fokker-Planck equation [36] to derive a *probability flow ODE* related to the SDE, which possesses the same marginal distribution at any given time  $t$  as the SDE. Specifically, the reverse process ODE derived from Eq. (3) can be expressed as:

$$dx_t = \left[ f(t)x_t - \frac{1}{2}g^2(t)\nabla_x \log q_t(x_t) \right] dt, \quad x_T \sim q(x_T). \quad (5)$$

Unlike SDE, ODE avoids the introduction of randomness, thereby allowing convergence to the data distribution in fewer time steps. Song et al. [4] employed a high-order RK45 ODE solver [37], achieving sample quality comparable to SDE at 1000 NFE with only 60 NFE. Furthermore, research such as DDIM [20] and DPM-Solver [21] explored discrete ODE forms capable of converging in fewer NFE. For DDIM, it breaks the Markov chain constraint on the basis of DDPM, deriving a new sampling formula expressed as follows:

$$x_{t-1} = \sqrt{\alpha_{t-1}} \left( \frac{x_t - \sqrt{1 - \alpha_t}\epsilon_\theta(x_t, t)}{\sqrt{\alpha_t}} \right) + \sqrt{1 - \alpha_{t-1} - \bar{\sigma}_t^2}\epsilon_\theta(x_t, t) + \bar{\sigma}_t\epsilon_t, \quad (6)$$

where  $\bar{\sigma}_t = \eta\sqrt{(1 - \alpha_{t-1})/(1 - \alpha_t)}\sqrt{1 - \alpha_t/\alpha_{t-1}}$ , and  $\alpha_t$  corresponds to  $\alpha_t^2$  in Eq. (1). When  $\eta = 1$ , Eq. (6) becomes a form of DDPM [2]; when  $\eta = 0$ , it degenerates into an ODE, the form adopted by DDIM [20], which can obtain high-quality samples in fewer time steps.

**Remark 1.** In this paper, we regard the gradient  $d\bar{x}_t$ , the noise network output  $\epsilon_\theta(x_t, t)$ , and the score function  $\nabla_x \log q_t(x_t)$  as expressing equivalent concepts. This is because Song et al. [4] demonstrated that  $\epsilon_\theta(x_t, t) = -\sigma_t\nabla_x \log q_t(x_t)$ . Moreover, we have discovered that any first-order solver of DPMs can be parameterized as  $x_{t-1} = \bar{x}_t - \gamma_t d\bar{x}_t + \xi\epsilon_t$ . Taking DDIM [20] as an example, where  $\bar{x}_t = \sqrt{\frac{\alpha_{t-1}}{\alpha_t}}x_t$ ,  $\gamma_t = \sqrt{\frac{\alpha_{t-1}}{\alpha_t} - \alpha_{t-1} - \sqrt{1 - \alpha_{t-1}}}$ ,  $d\bar{x}_t = \epsilon_\theta(x_t, t)$ , and  $\xi = 0$ . This indicates the similarity between SGD and the sampling process of DPMs, a discovery also implicitly suggested in the research of Xue et al. [31] and Wang et al. [38].

## 3 Method

### 3.1 Solving for reverse process diffusion ODEs

By substituting  $\epsilon_\theta(x_t, t) = -\sigma_t\nabla_x \log q_t(x_t)$  [4], Eq. (5) can be rewritten as:

$$\frac{dx_t}{dt} = s(\epsilon_\theta(x_t, t), x_t, t) := f(t)x_t + \frac{g^2(t)}{2\sigma_t}\epsilon_\theta(x_t, t), \quad x_T \sim q(x_T). \quad (7)$$

Given an initial value  $x_T$ , we define the time steps  $\{t_i\}_{i=0}^T$  to progressively decrease from  $t_0 = T$  to  $t_T = 0$ . Let  $\tilde{x}_{t_0} = x_T$  be the initial value. Using  $T$  steps of iteration, we compute the sequence  $\{\tilde{x}_{t_i}\}_{i=0}^T$  to obtain the solution of this ODE. By integrating both sides of Eq. (7), we can obtain the exact solution of this sampling ODE.

$$\tilde{x}_{t_i} = \tilde{x}_{t_{i-1}} + \int_{t_{i-1}}^{t_i} s(\epsilon_\theta(x_t, t), x_t, t) dt. \quad (8)$$

For any  $p$ -order ODE solver, Eq. (8) can be discretely represented as:

$$\tilde{x}_{t_{i-1} \rightarrow t_i} \approx \phi(Q, \tilde{x}_{t_{i-1}}, t_{i-1}, t_i) := \tilde{x}_{t_{i-1}} + \sum_{n=0}^{p-1} h(\epsilon_\theta(\tilde{x}_{\hat{t}_n}, \hat{t}_n), \tilde{x}_{\hat{t}_n}, \hat{t}_n) \cdot \Delta \hat{t}, \quad i \in [1, \dots, T]. \quad (9)$$

Here,  $Q = \left( \{\epsilon_\theta(\tilde{x}_{\hat{t}_n}, \hat{t}_n)\}_{n=0}^{p-1}, t_{i-1}, t_i \right)$  stores the set of  $p$  gradients computed over the intervals  $t_{i-1}$  and  $t_i$ . Specifically, when  $p = 1$ ,  $Q = \epsilon_\theta(\tilde{x}_{t_{i-1}}, t_{i-1})$ . The function  $\phi$  is any  $p$ -order ODE solver that updates the current state  $\tilde{x}_{t_{i-1}}$  from time point  $t_{i-1}$  to  $t_i$ , using the gradients stored in  $Q$ . The function  $h$  represents the way in which different  $p$ -order ODE solvers handle the function  $s$ , and its specific form depends on the solver’s design. For example, in the DPM-Solver [21], an exponential integrator is used to transform  $s$  into  $h$  in order to eliminate linear terms. In the case of a first-order Euler-Maruyama solver [39], it serves as an identity mapping of  $s$ .

When using the ODE solver defined in Eq. (9) for sampling, the choice of  $T = 1000$  leads to significant inefficiencies in DPMs. The study on DDIM [20] first revealed that by constructing a new forward sub-state sequence of length  $M + 1$  ( $M \leq T$ ),  $\{\tilde{x}_{t_i}\}_{i=0}^M$ , from a subsequence of time steps  $[0, \dots, T]$  and reversing this sub-state sequence, it is possible to converge to the data distribution in fewer time steps. However, as illustrated in Fig. 2a, for ODE solvers, as the time step size  $\Delta t = t_i - t_{i-1}$  increases, the gradient direction changes slowly initially, but undergoes abrupt changes as  $\Delta t \rightarrow T$ . This phenomenon indicates that under minimal NFE (i.e., maximal time step size  $\Delta t$ ) conditions, the discretization error in Eq. (9) is significantly amplified. Consequently, existing ODE solvers, when sampling under minimal NFE, must sacrifice sampling quality to gain speed, making it an extremely challenging task to reduce NFE to below 10 [21, 22]. Given this, we aim to develop an efficient timestep-skipping sampling algorithm, which reduces NFE while correcting discretization errors, thereby ensuring that sampling quality is not compromised, and may even be improved.

### 3.2 Sampling guided by past gradients

As illustrated in Fig. 2a, when the time step size  $\Delta t$  (i.e.,  $t_i - t_{i-1}$ ) is not excessively large, the MSE of the noise network, defined as  $\frac{1}{T-\Delta t} \sum_{t=0}^{T-\Delta t-1} \|\epsilon_\theta(x_t, t) - \epsilon_\theta(x_{t+\Delta t}, t + \Delta t)\|^2$ , is remarkably similar. This phenomenon is especially pronounced in ODE-based sampling algorithms, such as DDIM [20] and DPM-Solver [21]. This observation suggests that there are many unnecessary time steps in ODE-based sampling methods during the complete sampling process (e.g., when  $T = 1000$ ), which is one of the reasons these methods can generate samples in fewer steps. Based on this, we propose replacing the noise network of the current timestep with the output from a previous timestep to reduce unnecessary NFE without compromising the quality of the final generated samples.

Specifically, For any  $p$ -order ODE solver  $\phi$ , the sampling process from  $\tilde{x}_{t_{i-1}}$  to  $\tilde{x}_{t_i}$  can be reformulated according to Eq. (9) as follows:

$$\tilde{x}_{t_i} \approx \phi(\{\epsilon_\theta(\tilde{x}_{\hat{t}_n}, \hat{t}_n)\}_{n=0}^{p-1}, \tilde{x}_{t_{i-1}}, t_{i-1}, t_i). \quad (10)$$

Then, we store the noise network output in a *buffer* for use in the next timestep, as follows:

$$Q \stackrel{\text{buffer}}{\leftarrow} \left( \{\epsilon_\theta(\tilde{x}_{\hat{t}_n}, \hat{t}_n)\}_{n=0}^{p-1}, t_{i-1}, t_i \right), \quad (11)$$

where  $t_{i-1}$  and  $t_i$  represent the intervals over which the set of  $p$  gradients are computed. For the sampling process from  $\tilde{x}_{t_i}$  to  $\tilde{x}_{t_{i+1}}$ , we directly use the noise network output saved in the buffer from the previous timestep to replace the current timestep’s noise network, thereby updating the intermediate states to the next timestep (i.e., the “springboard”  $\tilde{x}_{t_{i+1}}$ ), as detailed below:

$$\tilde{x}_{t_{i+1}} \approx \phi(Q, \tilde{x}_{t_i}, t_i, t_{i+1}), \quad \text{where } Q = \left( \{\epsilon_\theta(\tilde{x}_{\hat{t}_n}, \hat{t}_n)\}_{n=0}^{p-1}, t_{i-1}, t_i \right). \quad (12)$$

By using this approach, we can reduce unnecessary NFE, thereby accelerating the sampling process.

**Remark 2.** *Notably, when the time step size  $\Delta t$  is very large ( $NFE < 10$ ), the similarity between past and current gradients decreases sharply, making “springboard”  $\tilde{x}_{t_{i+1}}$  unreliable in Eq. (12). Therefore, in Sec. 3.3, we use  $\tilde{x}_{t_{i+1}}$  solely to predict a foresight update direction (i.e., future gradient) to reduce errors caused by the replacement, as shown in Fig. 2b and Fig. 2c. Both past and future gradients are complementary and indispensable, as demonstrated by the ablation study in Sec. 4.3.*

### 3.3 Sampling guided by future gradients

As stated in Remark 1, considering the similarities between the sampling process of DPMs and SGD [34], we introduce a *foresight* update mechanism of Nesterov momentum, utilizing future

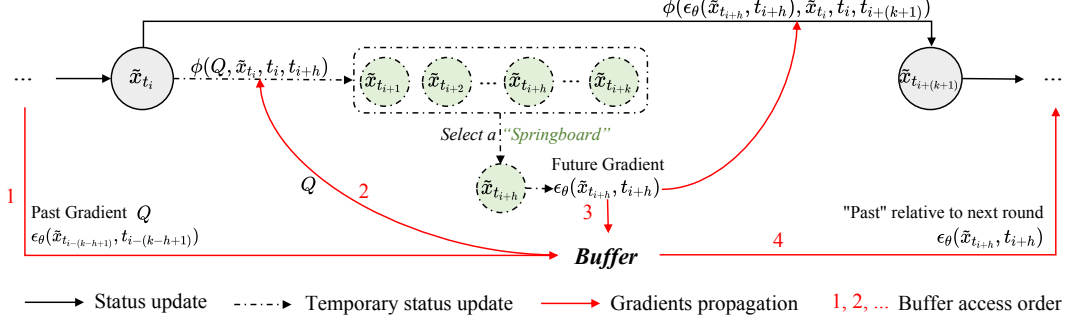


Figure 3: Illustration of a single iteration update of PFDiff- $k_h$  combined with any first-order ODE solver  $\phi$ . Given specific values of  $k$  and  $h$  ( $k \leq 3$  ( $h \leq k$ )), PFDiff first uses the past gradient  $Q$  stored in the Buffer from the previous iteration to replace the current gradient, updating to the “springboard”  $x_{t_{i+h}}$ ; then the future gradient is calculated using the “springboard”; finally, the future gradient is used to replace the current gradient, completing a full update iteration. The future gradient will also be passed to the next iteration as the “past” gradient for the next round of updates.

gradient information to assist the current intermediate state in achieving more efficient leapfrog updates. Specifically, for the sampling process from  $\tilde{x}_{t_i}$  to  $\tilde{x}_{t_{i+2}}$ , we consider using future gradients (corresponding to time point  $t_{i+1}$ ) to replace the current gradients (corresponding to  $t_i$ ). Continuing from Eq. (12), we estimate the future gradient using the “springboard”  $\tilde{x}_{t_{i+1}}$  and update the buffer as follows:

$$Q \xleftarrow{\text{buffer}} \left( \{ \epsilon_\theta(\tilde{x}_{\hat{t}_n}, \hat{t}_n) \}_{n=0}^{p-1}, t_{i+1}, t_{i+2} \right). \quad (13)$$

Subsequently, leveraging the concept of foresight updates, we predict a further future intermediate state  $\tilde{x}_{t_{i+2}}$  using the current intermediate state  $\tilde{x}_{t_i}$  along with the future gradient corresponding to time point  $t_{i+1}$ , as shown below:

$$\tilde{x}_{t_{i+2}} \approx \phi(Q, \tilde{x}_{t_i}, t_i, t_{i+2}), \quad \text{where } Q = \left( \{ \epsilon_\theta(\tilde{x}_{\hat{t}_n}, \hat{t}_n) \}_{n=0}^{p-1}, t_{i+1}, t_{i+2} \right). \quad (14)$$

Furthermore, we analyze how to correct the errors of the first-order ODE solvers in the discretized Eq. (8) using future gradients. Let  $s_\theta(x_t, t) := s(\epsilon_\theta(x_t, t), x_t, t)$ , we further analyze the term from Eq. (8) that may cause errors,  $\int_{t_{i-1}}^{t_i} s_\theta(x_t, t) dt$ . Assuming that  $s_\theta^{(n)}(x_r, r)$ ,  $r \in [t_{i-1}, t_i]$  exists and is continuous, applying Taylor’s expansion at  $t = r$ , we derive:

$$\begin{aligned} \int_{t_{i-1}}^{t_i} s_\theta(x_t, t) dt &= \int_{t_{i-1}}^{t_i} \left[ \sum_{n=0}^{\infty} \frac{s_\theta^{(n)}(x_r, r)}{n!} (t-r)^n + R_n(t) \right] dt \\ &\approx \int_{t_{i-1}}^{t_i} \left[ \sum_{n=0}^{\infty} \frac{s_\theta^{(n)}(x_r, r)}{n!} (t-r)^n \right] dt \\ &= \sum_{n=0}^{\infty} \frac{(t_i - r)^{n+1} - (t_{i-1} - r)^{n+1}}{(n+1)!} s_\theta^{(n)}(x_r, r) \\ &= s_\theta(x_r, r) (t_i - t_{i-1}) + \underbrace{\sum_{n=1}^{\infty} \frac{(t_i - r)^{n+1} - (t_{i-1} - r)^{n+1}}{(n+1)!} s_\theta^{(n)}(x_r, r)}_{\text{“higher-order derivative terms”}}. \end{aligned} \quad (15)$$

**Proposition 3.1.** For any given DPM first-order ODE solver, the absolute values of the coefficients for higher-order derivative terms in Eq. (15) are smaller when using the future time point  $r = \varepsilon$  gradient compared to the current time point  $r = t_{i-1}$  gradient, as follows (Proof in Appendix B.2):

$$\left| \frac{(t_i - \varepsilon)^n - (t_{i-1} - \varepsilon)^n}{n!} \right| < \left| \frac{(t_i - t_{i-1})^n}{n!} \right|, \quad \text{where } \varepsilon \in (t_{i-1}, t_i), n \geq 2. \quad (16)$$

Proposition 3.1 indicates that neglecting higher-order derivative terms has less impact when sampling with future gradients, correcting for the discretization errors inherent in first-order ODE

solvers. However, higher-order ODE solvers approximate higher-order derivative terms by estimating the noise network’s output multiple times [21, 22, 27]. Future gradients and higher-order ODE solvers reduce the discretization errors caused by neglecting higher-order derivative terms in two parallel manners, complicating the error analysis when both methods are used simultaneously. Therefore, when using higher-order ODE solvers as a baseline, the sampling process is accelerated by only using past gradients. It is only necessary to modify Eq. (14) to  $\tilde{x}_{t_{i+2}} \approx \phi(Q, \tilde{x}_{t_{i+1}}, t_{i+1}, t_{i+2})$  while keeping  $Q$  constant.

### 3.4 PFDiff: sampling guided by past and future gradients

Combining Sec. 3.2 and Sec. 3.3, the “springboard”  $\tilde{x}_{t_{i+1}}$  obtained through Eq. (12) is used to update the buffer  $Q$  in Eq. (13). In this way, we achieve our proposed efficient timestep-skipping algorithm, which we name PFDiff. Notably, during the iteration from intermediate state  $\tilde{x}_{t_i}$  to  $\tilde{x}_{t_{i+2}}$ , we only perform a single batch computation (NFE =  $p$ ) of the noise network in Eq. (13). Furthermore, we propose that in a single iteration process,  $\tilde{x}_{t_{i+2}}$  in Eq. (14) can be modified to  $\tilde{x}_{t_{i+(k+1)}}$ , achieving a  $k$ -step skip to sample more distant future intermediate states. Also, when  $k \neq 1$ , the buffer  $Q$  from Eq. (13) has various computational origins. This can be accomplished by modifying “springboard”  $\tilde{x}_{t_{i+1}}$  in Eq. (12) to  $\tilde{x}_{t_{i+h}}$ . We collectively refer to this multi-step skipping and different “springboard” selection strategy as PFDiff- $k$ - $h$  ( $l \leq h$ ). The algorithmic process is illustrated in Fig. 3 and Algorithm 1, with further details provided in Appendix C. Additionally, through the comparison of sampling trajectories between PFDiff-1 and a first-order ODE sampler, as shown in Fig. 2c, PFDiff-1 showcases its capability to correct the sampling trajectory of the first-order ODE sampler while reducing the NFE. Meanwhile, we observed that PFDiff completes two updates with just one gradient computation (1 NFE), which is equivalent to achieving an update process of a second-order ODE solver with 2 NFE. This effectiveness is derived from PFDiff’s *information-efficient* update process, which utilizes both past and future gradients that are complementary and indispensable. The convergence of PFDiff’s sampling outcomes to the data distribution consistent with solver  $\phi$  relies on the *Mean Value Theorem*, as detailed in Appendix B.3.

## 4 Experiments

In this section, we validate the effectiveness of PFDiff as an *orthogonal* and *training-free* sampler through a series of extensive experiments. This sampler can be integrated with any order of ODE solvers, thereby significantly enhancing the sampling efficiency of various types of pre-trained DPMs. To systematically showcase the performance of PFDiff, we categorize the pre-trained DPMs into two main types: conditional and unconditional. Unconditional DPMs are further subdivided

---

#### Algorithm 1 PFDiff-1

---

**Require:** initial value  $x_T$ , NFE  $N$ , model  $\epsilon_\theta$ , any  $p$ -order solver  $\phi$

- 1: Define time steps  $\{t_i\}_{i=0}^M$  with  $M = 2N - 1p$
- 2:  $\tilde{x}_{t_0} \leftarrow x_T$
- 3:  $Q \leftarrow^{\text{buffer}} \left( \{\epsilon_\theta(\tilde{x}_{\hat{t}_n}, \hat{t}_n)\}_{n=0}^{p-1}, t_0, t_1 \right)$  ▷ Initialize buffer
- 4:  $\tilde{x}_{t_1} = \phi(Q, \tilde{x}_{t_0}, t_0, t_1)$
- 5: **for**  $i \leftarrow 1$  to  $\frac{M}{p} - 2$  **do**
- 6:     **if**  $(i - 1) \bmod 2 = 0$  **then**
- 7:          $\tilde{x}_{t_{i+1}} = \phi(Q, \tilde{x}_{t_i}, t_i, t_{i+1})$  ▷ Updating guided by past gradients
- 8:          $Q \leftarrow^{\text{buffer}} \left( \{\epsilon_\theta(\tilde{x}_{\hat{t}_n}, \hat{t}_n)\}_{n=0}^{p-1}, t_{i+1}, t_{i+2} \right)$  ▷ Update buffer (overwrite)
- 9:         **if**  $p = 1$  **then**
- 10:              $\tilde{x}_{t_{i+2}} = \phi(Q, \tilde{x}_{t_i}, t_i, t_{i+2})$  ▷ Anticipatory updating guided by future gradients
- 11:         **else if**  $p > 1$  **then**
- 12:              $\tilde{x}_{t_{i+2}} = \phi(Q, \tilde{x}_{t_{i+1}}, t_{i+1}, t_{i+2})$  ▷ The higher-order solver uses only past gradients
- 13:         **end if**
- 14:     **end if**
- 15: **end for**
- 16: **return**  $\tilde{x}_{t_M}$

---



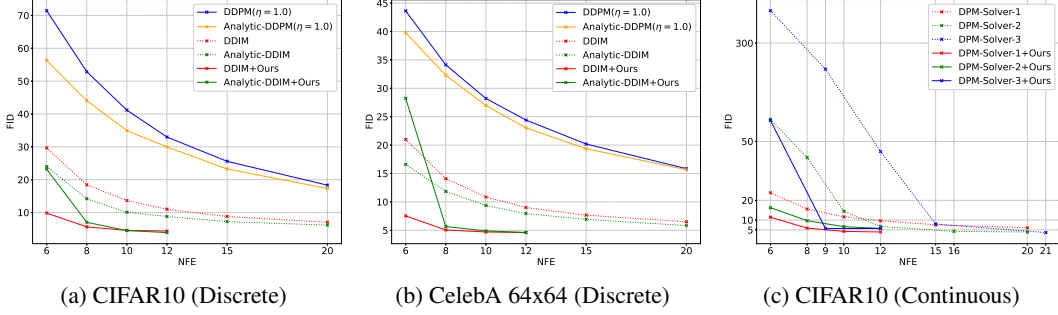


Figure 4: Unconditional sampling results. We report the  $FID_{\downarrow}$  for different methods by varying the number of function evaluations (NFE), evaluated on 50k samples.

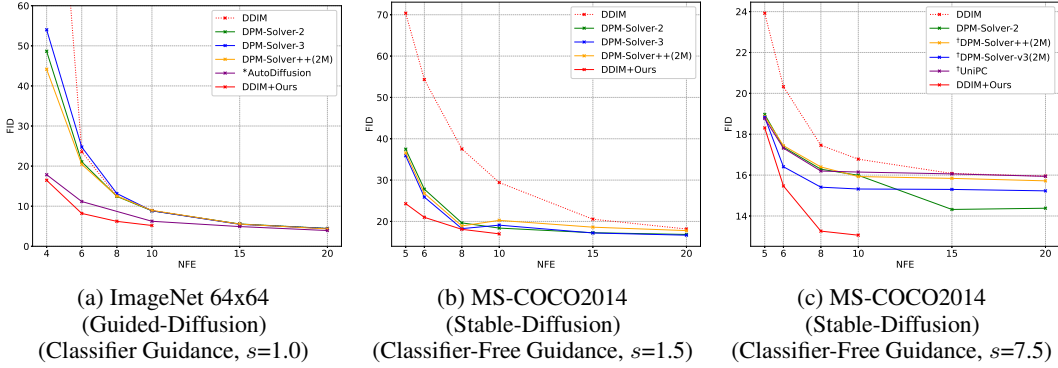


Figure 5: Conditional sampling results. We report the  $FID_{\downarrow}$  for different methods by varying the NFE. Evaluated: ImageNet 64x64 with 50k, others with 10k samples. \* AutoDiffusion [26] method requires additional search costs. <sup>†</sup>We borrow the results reported in DPM-Solver-v3 [27] directly.

into discrete and continuous, while conditional DPMs are subdivided into classifier guidance and classifier-free guidance. In choosing ODE solvers, we utilized the widely recognized first-order DDIM [20], Analytic-DDIM [23], and the higher-order DPM-Solver [21] as baselines. For each experiment, we use the Fréchet Inception Distance ( $FID_{\downarrow}$ ) [40] as the primary evaluation metric, and provide the experimental results of the Inception Score ( $IS_{\uparrow}$ ) [41] in the Appendix D.7 for reference. Lastly, apart from the ablation studies on parameters  $k$  and  $h$  discussed in Sec. 4.3, we showcase the optimal results of PFDiff- $k_h$  (where  $k = 1, 2, 3$  and  $h \leq k$ ) across six configurations as a performance demonstration of PFDiff. As described in Appendix C, this does not increase the computational burden in practical applications. All experiments were conducted on an NVIDIA RTX 3090 GPU.

#### 4.1 Unconditional sampling

For unconditional DPMs, we selected discrete DDPM [2] and DDIM [20], as well as pre-trained models from continuous ScoreSDE [4], to assess the effectiveness of PFDiff. For these pre-trained models, all experiments sampled 50k samples to compute evaluation metrics.

For unconditional discrete DPMs, we first select first-order ODE solvers DDIM [20] and Analytic-DDIM [23] as baselines, while implementing SDE-based DDPM [2] and Analytic-DDPM [23] methods for comparison, where  $\eta = 1.0$  is from  $\bar{\sigma}_t$  in Eq. (6). We conduct experiments on the CIFAR10 [42] and CelebA 64x64 [43] datasets using the quadratic time steps employed by DDIM. By varying the NFE from 6 to 20, the evaluation metric  $FID_{\downarrow}$  is shown in Figs. 4a and 4b. Additionally, experiments with uniform time steps are conducted on the CelebA 64x64, LSUN-bedroom 256x256 [44], and LSUN-church 256x256 [44] datasets, with more results available in Appendix D.2. Our experimental results demonstrate that PFDiff, based on pre-trained models of discrete unconditional DPMs, significantly improves the sampling efficiency of DDIM and Analytic-DDIM samplers across multiple datasets. For instance, on the CIFAR10 dataset, PFDiff combined with DDIM achieves a  $FID$



of 4.10 with only 15 NFE, comparable to DDIM’s performance of 4.04 FID with 1000 NFE. This is something other time-step skipping algorithms [23, 28] that sacrifice sampling quality for speed cannot achieve. Furthermore, in Appendix D.2, by varying  $\eta$  from 1.0 to 0.0 in Eq. (6) to control the scale of noise introduced by SDE, we observe that as  $\eta$  decreases (reducing noise introduction), the performance of PFDiff gradually improves. This is consistent with the trend shown in Fig. 2a, where reducing noise introduction leads to an improvement in the similarity of the model’s outputs.

For unconditional continuous DPMs, we choose the DPM-Solver-1, -2 and -3 [21] as the baseline to verify the effectiveness of PFDiff as an orthogonal timestep-skipping algorithm on the first and higher-order ODE solvers. We conducted experiments on the CIFAR10 [42] using quadratic time steps, varying the NFE. The experimental results using FID $\downarrow$  as the evaluation metric are shown in Fig. 4c. More experimental details can be found in Appendix D.3. We observe that PFDiff consistently improves the sampling performance over the baseline with fewer NFE settings, particularly in cases where higher-order ODE solvers fail to converge with a small NFE (below 10) [21].

## 4.2 Conditional sampling

For conditional DPMs, we selected the pre-trained models of the widely recognized classifier guidance paradigm, ADM-G [5], and the classifier-free guidance paradigm, Stable-Diffusion [9], to validate the effectiveness of PFDiff. We employed uniform time steps setting and the DDIM [20] ODE solver as a baseline across all datasets. Evaluation metrics were computed by sampling 50k samples on the ImageNet 64x64 [33] dataset for ADM-G and 10k samples on other datasets, including ImageNet 256x256 [33] in ADM-G and MS-COCO2014 [32] in Stable-Diffusion.

For conditional DPMs employing the classifier guidance paradigm, we conducted experiments on the ImageNet 64x64 dataset [33] with a guidance scale ( $s$ ) set to 1.0. For comparison, we implemented DPM-Solver-2 and -3 [21], and DPM-Solver++(2M) [22], which exhibit the best performance on conditional DPMs. Additionally, we introduced the AutoDiffusion method [26] using DDIM as a baseline for comparison, noting that this method incurs additional search costs. We compared FID $\downarrow$  scores by varying the NFE as depicted in Fig. 5a, with corresponding visual comparisons shown in Fig. 1b. We observed that PFDiff reduced the FID from 138.81 with 4 NFE in DDIM to 16.46, achieving an 88.14% improvement in quality. The visual results in Fig. 1b further demonstrate that, at the same NFE setting, PFDiff achieves higher-quality sampling. Furthermore, we evaluated PFDiff’s sampling performance based on DDIM on the large-scale ImageNet 256x256 dataset [33]. Detailed results are provided in Appendix D.4.

For conditional, classifier-free guidance paradigms of DPMs, we employed the sd-v1-4 checkpoint and computed the FID $\downarrow$  scores on the validation set of MS-COCO2014 [32]. We conducted experiments with a guidance scale ( $s$ ) set to 7.5 and 1.5. For comparison, we implemented DPM-Solver-2 and -3 [21], and DPM-Solver++(2M) [22] methods. At  $s = 7.5$ , we introduced the state-of-the-art method reported in DPM-Solver-v3 [27] for comparison, along with DPM-Solver++(2M) [22], UniPC [30], and DPM-Solver-v3(2M) [27]. The FID $\downarrow$  metrics by varying the NFE are presented in Figs. 5b and 5c, with additional visual results illustrated in Fig. 1a. We observed that PFDiff, solely based on DDIM, achieved state-of-the-art results during the sampling process of Stable-Diffusion, thus demonstrating the efficacy of PFDiff. Further experimental details can be found in Appendix D.5.

## 4.3 Ablation study

We conducted ablation experiments on the six different algorithm configurations of PFDiff mentioned in Appendix C, with  $k = 1, 2, 3$  ( $h \leq k$ ). Specifically, we evaluated the FID $\downarrow$  scores on the unconditional and conditional pre-trained DPMs [2, 5]. Detailed experimental setups and results can be found in Appendix D.6.1. The experimental results indicate that for various pre-trained DPMs, the choice of parameters  $k$  and  $h$  is not critical, as most combinations of  $k$  and  $h$  within PFDiff can enhance the sampling efficiency over the baseline. Moreover, with  $k = 2$  and  $h = 1$  fixed, PFDiff-2\_1 can always improve the baseline’s sampling quality within the range of 4~20 NFE. For even better sampling quality, one can sample a small subset of examples (e.g., 5k) to compute evaluation metrics or directly conduct visual analysis, easily identifying the most effective  $k$  and  $h$  combinations.

To validate the effectiveness of PFDiff, a key factor is its information-efficient update process, which utilizes past and future gradients that are complementary and indispensable to jointly guide first-order ODE solvers. We employ DDIM [20] as the baseline, removing past and future gradients separately. Moreover, we introduce methods [28] that cache part of past gradients for comparison. As shown in Appendix D.6.2, experimental results indicate that only past (including cache) or only future gradients can slightly improve sampling performance, but their combination (i.e., the complete PFDiff) significantly enhances the performance of first-order ODE solvers, especially with very few NFE ( $<10$ ). Additionally, we provide experimental results on inference time in Appendix D.6.2, revealing that methods [28] that cache part of past gradients not only incur additional inference costs but also exhibit relatively weak acceleration effects with few NFE ( $<10$ ). However, PFDiff and the used baseline have consistent inference times and exhibit significantly accelerated effects, further validating its effectiveness.

## 5 Conclusion

In this paper, based on the recognition that the ODE solvers of DPMs exhibit significant similarity in model outputs when the time step size is not excessively large, and with the aid of a foresight update mechanism, we propose PFDiff, a novel method that leverages the gradient guidance from both past and future to rapidly update the current intermediate state. This approach effectively reduces the unnecessary number of function evaluations (NFE) in the ODE solvers and significantly corrects the errors of first-order ODE solvers during the sampling process. Extensive experiments demonstrate the orthogonality and effectiveness of PFDiff on both unconditional and conditional pre-trained DPMs, especially in conditional pre-trained DPMs where PFDiff outperforms previous state-of-the-art training-free sampling methods.

**Limitations and broader impact** Although PFDiff can effectively accelerate the sampling speed of existing ODE solvers, it still lags behind the sampling speed of training-based acceleration methods and one-step generation paradigms such as GANs. Moreover, there is no universal setting for the optimal combination of parameters  $k$  and  $h$  in PFDiff; adjustments are required according to different pre-trained DPMs and NFE. It is noteworthy that PFDiff may be utilized to accelerate the generation of malicious content, thereby having a detrimental impact on society.

## References

- [1] Jascha Sohl-Dickstein, Eric Weiss, Niru Maheswaranathan, and Surya Ganguli. Deep unsupervised learning using nonequilibrium thermodynamics. In *International conference on machine learning*, pages 2256–2265. PMLR, 2015.
- [2] Jonathan Ho, Ajay Jain, and Pieter Abbeel. Denoising diffusion probabilistic models. *Advances in neural information processing systems*, 33:6840–6851, 2020.
- [3] Yang Song and Stefano Ermon. Generative modeling by estimating gradients of the data distribution. *Advances in neural information processing systems*, 32, 2019.
- [4] Yang Song, Jascha Sohl-Dickstein, Diederik P Kingma, Abhishek Kumar, Stefano Ermon, and Ben Poole. Score-based generative modeling through stochastic differential equations. *arXiv preprint arXiv:2011.13456*, 2020.
- [5] Prafulla Dhariwal and Alexander Nichol. Diffusion models beat gans on image synthesis. *Advances in neural information processing systems*, 34:8780–8794, 2021.
- [6] Jonathan Ho, Chitwan Saharia, William Chan, David J Fleet, Mohammad Norouzi, and Tim Salimans. Cascaded diffusion models for high fidelity image generation. *Journal of Machine Learning Research*, 23(47):1–33, 2022.
- [7] William Peebles and Saining Xie. Scalable diffusion models with transformers. In *Proceedings of the IEEE/CVF International Conference on Computer Vision*, pages 4195–4205, 2023.
- [8] Mostafa Dehghani, Basil Mustafa, Josip Djolonga, Jonathan Heek, Matthias Minderer, Mathilde Caron, Andreas Steiner, Joan Puigcerver, Robert Geirhos, Ibrahim M Alabdulmohsin, et al. Patch n’pack: Navit, a vision transformer for any aspect ratio and resolution. *Advances in Neural Information Processing Systems*, 36, 2024.

- [9] Robin Rombach, Andreas Blattmann, Dominik Lorenz, Patrick Esser, and Björn Ommer. High-resolution image synthesis with latent diffusion models. In *Proceedings of the IEEE/CVF conference on computer vision and pattern recognition*, pages 10684–10695, 2022.
- [10] James Betker, Gabriel Goh, Li Jing, Tim Brooks, Jianfeng Wang, Linjie Li, Long Ouyang, Juntang Zhuang, Joyce Lee, Yufei Guo, et al. Improving image generation with better captions. *Computer Science*. <https://cdn.openai.com/papers/dall-e-3.pdf>, 2(3):8, 2023.
- [11] Kaitao Song, Yichong Leng, Xu Tan, Yicheng Zou, Tao Qin, and Dongsheng Li. Transcormer: Transformer for sentence scoring with sliding language modeling. *Advances in Neural Information Processing Systems*, 35:11160–11174, 2022.
- [12] Ben Poole, Ajay Jain, Jonathan T Barron, and Ben Mildenhall. Dreamfusion: Text-to-3d using 2d diffusion. *arXiv preprint arXiv:2209.14988*, 2022.
- [13] Chen-Hsuan Lin, Jun Gao, Luming Tang, Towaki Takikawa, Xiaohui Zeng, Xun Huang, Karsten Kreis, Sanja Fidler, Ming-Yu Liu, and Tsung-Yi Lin. Magic3d: High-resolution text-to-3d content creation. In *Proceedings of the IEEE/CVF Conference on Computer Vision and Pattern Recognition*, pages 300–309, 2023.
- [14] Ian Goodfellow, Jean Pouget-Abadie, Mehdi Mirza, Bing Xu, David Warde-Farley, Sherjil Ozair, Aaron Courville, and Yoshua Bengio. Generative adversarial nets. *Advances in neural information processing systems*, 27, 2014.
- [15] Diederik P Kingma and Max Welling. Auto-encoding variational bayes. *arXiv preprint arXiv:1312.6114*, 2013.
- [16] Tim Salimans and Jonathan Ho. Progressive distillation for fast sampling of diffusion models. *arXiv preprint arXiv:2202.00512*, 2022.
- [17] Xingchao Liu, Chengyue Gong, and Qiang Liu. Flow straight and fast: Learning to generate and transfer data with rectified flow. *arXiv preprint arXiv:2209.03003*, 2022.
- [18] Zhendong Wang, Huangjie Zheng, Pengcheng He, Weizhu Chen, and Mingyuan Zhou. Diffusion-gan: Training gans with diffusion. *arXiv preprint arXiv:2206.02262*, 2022.
- [19] Yang Song, Prafulla Dhariwal, Mark Chen, and Ilya Sutskever. Consistency models. *arXiv preprint arXiv:2303.01469*, 2023.
- [20] Jiaming Song, Chenlin Meng, and Stefano Ermon. Denoising diffusion implicit models. *arXiv preprint arXiv:2010.02502*, 2020.
- [21] Cheng Lu, Yuhao Zhou, Fan Bao, Jianfei Chen, Chongxuan Li, and Jun Zhu. Dpm-solver: A fast ode solver for diffusion probabilistic model sampling in around 10 steps. *Advances in Neural Information Processing Systems*, 35:5775–5787, 2022.
- [22] Cheng Lu, Yuhao Zhou, Fan Bao, Jianfei Chen, Chongxuan Li, and Jun Zhu. Dpm-solver++: Fast solver for guided sampling of diffusion probabilistic models. *arXiv preprint arXiv:2211.01095*, 2022.
- [23] Fan Bao, Chongxuan Li, Jun Zhu, and Bo Zhang. Analytic-dpm: an analytic estimate of the optimal reverse variance in diffusion probabilistic models. *arXiv preprint arXiv:2201.06503*, 2022.
- [24] Fan Bao, Chongxuan Li, Jiacheng Sun, Jun Zhu, and Bo Zhang. Estimating the optimal covariance with imperfect mean in diffusion probabilistic models. *arXiv preprint arXiv:2206.07309*, 2022.
- [25] Luping Liu, Yi Ren, Zhijie Lin, and Zhou Zhao. Pseudo numerical methods for diffusion models on manifolds. *arXiv preprint arXiv:2202.09778*, 2022.
- [26] Lijiang Li, Huixia Li, Xiawu Zheng, Jie Wu, Xuefeng Xiao, Rui Wang, Min Zheng, Xin Pan, Fei Chao, and Rongrong Ji. Autodiffusion: Training-free optimization of time steps and architectures for automated diffusion model acceleration. In *Proceedings of the IEEE/CVF International Conference on Computer Vision*, pages 7105–7114, 2023.
- [27] Kaiwen Zheng, Cheng Lu, Jianfei Chen, and Jun Zhu. Dpm-solver-v3: Improved diffusion ode solver with empirical model statistics. *arXiv preprint arXiv:2310.13268*, 2023.
- [28] Xinyin Ma, Gongfan Fang, and Xinchao Wang. Deepcache: Accelerating diffusion models for free. In *Proceedings of the IEEE/CVF Conference on Computer Vision and Pattern Recognition*, pages 15762–15772, 2024.

- [29] Felix Wimbauer, Bichen Wu, Edgar Schoenfeld, Xiaoliang Dai, Ji Hou, Zijian He, Artsiom Sanakoyeu, Peizhao Zhang, Sam Tsai, Jonas Kohler, et al. Cache me if you can: Accelerating diffusion models through block caching. In *Proceedings of the IEEE/CVF Conference on Computer Vision and Pattern Recognition*, pages 6211–6220, 2024.
- [30] Wenliang Zhao, Lujia Bai, Yongming Rao, Jie Zhou, and Jiwen Lu. Unipc: A unified predictor-corrector framework for fast sampling of diffusion models. *Advances in Neural Information Processing Systems*, 36, 2024.
- [31] Shuchen Xue, Mingyang Yi, Weijian Luo, Shifeng Zhang, Jiacheng Sun, Zhenguo Li, and Zhi-Ming Ma. Sa-solver: Stochastic adams solver for fast sampling of diffusion models. *Advances in Neural Information Processing Systems*, 36, 2024.
- [32] Tsung-Yi Lin, Michael Maire, Serge Belongie, James Hays, Pietro Perona, Deva Ramanan, Piotr Dollár, and C Lawrence Zitnick. Microsoft coco: Common objects in context. In *Computer Vision—ECCV 2014: 13th European Conference, Zurich, Switzerland, September 6–12, 2014, Proceedings, Part V 13*, pages 740–755. Springer, 2014.
- [33] Jia Deng, Wei Dong, Richard Socher, Li-Jia Li, Kai Li, and Li Fei-Fei. Imagenet: A large-scale hierarchical image database. In *2009 IEEE conference on computer vision and pattern recognition*, pages 248–255. Ieee, 2009.
- [34] Herbert Robbins and Sutton Monro. A stochastic approximation method. *The annals of mathematical statistics*, pages 400–407, 1951.
- [35] Yurii Nesterov. A method of solving a convex programming problem with convergence rate  $o(1/k^{** 2})$ . *Doklady Akademii Nauk SSSR*, 269(3):543, 1983.
- [36] Bernt Øksendal and Bernt Øksendal. *Stochastic differential equations*. Springer, 2003.
- [37] John R Dormand and Peter J Prince. A family of embedded runge-kutta formulae. *Journal of computational and applied mathematics*, 6(1):19–26, 1980.
- [38] Kai Wang, Zhaopan Xu, Yukun Zhou, Zelin Zang, Trevor Darrell, Zhuang Liu, and Yang You. Neural network diffusion. *arXiv preprint arXiv:2402.13144*, 2024.
- [39] Peter E Kloeden, Eckhard Platen, Peter E Kloeden, and Eckhard Platen. *Stochastic differential equations*. Springer, 1992.
- [40] Martin Heusel, Hubert Ramsauer, Thomas Unterthiner, Bernhard Nessler, and Sepp Hochreiter. Gans trained by a two time-scale update rule converge to a local nash equilibrium. *Advances in neural information processing systems*, 30, 2017.
- [41] Tim Salimans, Ian Goodfellow, Wojciech Zaremba, Vicki Cheung, Alec Radford, and Xi Chen. Improved techniques for training gans. *Advances in neural information processing systems*, 29, 2016.
- [42] Alex Krizhevsky, Geoffrey Hinton, et al. Learning multiple layers of features from tiny images. 2009.
- [43] Ziwei Liu, Ping Luo, Xiaogang Wang, and Xiaoou Tang. Deep learning face attributes in the wild. In *Proceedings of the IEEE international conference on computer vision*, pages 3730–3738, 2015.
- [44] Fisher Yu, Ari Seff, Yinda Zhang, Shuran Song, Thomas Funkhouser, and Jianxiong Xiao. Lsun: Construction of a large-scale image dataset using deep learning with humans in the loop. *arXiv preprint arXiv:1506.03365*, 2015.
- [45] Elliott Ward Cheney, EW Cheney, and W Cheney. *Analysis for applied mathematics*, volume 1. Springer, 2001.
- [46] Zhenyu Zhou, Defang Chen, Can Wang, and Chun Chen. Fast ode-based sampling for diffusion models in around 5 steps. In *Proceedings of the IEEE/CVF Conference on Computer Vision and Pattern Recognition*, pages 7777–7786, 2024.

## A Related work

While the solvers for Diffusion Probabilistic Models (DPMs) are categorized into two types, SDE and ODE, most current accelerated sampling techniques are based on ODE solvers due to the observation that the stochastic noise introduced by SDE solvers hampers rapid convergence. ODE-based solvers are further divided into training-based methods [16–19] and training-free samplers [20–31]. Training-based methods can notably reduce the number of sampling steps required for DPMs. An example of such a method is the knowledge distillation algorithm proposed by Song et al. [19], which achieves one-step sampling for DPMs. This sampling speed is comparable to that of GANs [14] and VAEs [15]. However, these methods often entail significant additional costs for distillation training. This requirement poses a challenge when applying them to large pre-trained DPM models. Therefore, our work primarily focuses on training-free, ODE-based accelerated sampling strategies.

Training-free accelerated sampling techniques based on ODE can generally be applied in a plug-and-play manner, adapting to existing pre-trained DPMs. These methods can be categorized based on the order of the ODE solver—that is, the NFE required per sampling iteration—into first-order [20, 23–25] and higher-order [21, 22, 27, 30, 37]. Typically, higher-order ODE solvers tend to sample at a faster rate, but may fail to converge when the NFE is low (below 10), sometimes performing even worse than first-order ODE solvers. In addition, there are orthogonal techniques for accelerated sampling. For instance, Li et al. [26] build upon existing ODE solvers and use search algorithms to find optimal sampling sub-sequences and model structures to further speed up the sampling process; Ma et al. [28] and Wimbauer et al. [29] observe that the low-level features of noise networks at adjacent time steps exhibit similarities, and they use caching techniques to substitute some of the network’s low-level features, thereby further reducing the number of required time steps.

The algorithm we propose belongs to the class of training-free and orthogonal accelerated sampling techniques, capable of further accelerating the sampling process on the basis of existing first-order and higher-order ODE solvers. Compared to the aforementioned orthogonal sampling techniques, even though the skipping strategy proposed by Ma et al. [28] and Wimbauer et al. [29] effectively accelerates the sampling process, it may do so at the cost of reduced sampling quality, making it challenging to reduce the NFE below 50. Although Li et al. [26] can identify more optimal subsampling sequences and model structures, this implies higher search costs. In contrast, our proposed orthogonal sampling algorithm is more efficient in skipping time steps. First, our skipping strategy does not require extensive search costs. Second, we can correct the sampling trajectory of first-order ODE solvers while reducing the number of sampling steps required by existing ODE solvers, achieving more efficient accelerated sampling.

## B Proof of convergence and error correction for PFDiff

In this section, we first prove that neglecting higher-order derivative terms has a smaller impact on the first-ODE solvers when using future gradients (i.e., Proposition 3.1). Subsequently, we prove the convergence of PFDiff based on the *Mean Value Theorem* for Integrals.

### B.1 Assumptions

For PFDiff- $k\_h$  we make the following assumptions:

**Assumption B.1.** *The higher-order derivatives  $s_\theta^{(n)}(x_r, r)$  (as a function of  $r$ ), as defined in Eq. (15), where  $r \in [t_{i-1}, t_i]$  and  $n \geq 1$ , exist and are continuous.*

**Assumption B.2.** *When the time step size  $\Delta t = t_i - t_{i-(k-h+1)}$  is not excessively large, the output estimates of the noise network based on the  $p$ -order ODE solver at different time steps are approximately the same, that is,  $\left(\{\epsilon_\theta(\tilde{x}_{\hat{t}_n}, \hat{t}_n)\}_{n=0}^{p-1}, t_i, t_{i+h}\right) \approx \left(\{\epsilon_\theta(\tilde{x}_{\hat{t}_n}, \hat{t}_n)\}_{n=0}^{p-1}, t_{i-(k-h+1)}, t_i\right)$ .*

**Assumption B.3.** *For the integral from time step  $t_i$  to  $t_{i+(k+1)}$ ,  $\int_{t_i}^{t_{i+(k+1)}} s(\epsilon_\theta(x_t, t), x_t, t) dt$ , there exist intermediate time steps  $t_{\bar{s}}, t_s \in [t_i, t_{i+(k+1)}]$  such that  $\int_{t_i}^{t_{i+(k+1)}} s(\epsilon_\theta(x_t, t), x_t, t) dt = s(\epsilon_\theta(x_{t_{\bar{s}}}, t_{\bar{s}}), x_{t_{\bar{s}}}, t_{\bar{s}}) \cdot (t_{i+(k+1)} - t_i) = h(\epsilon_\theta(x_{t_s}, t_s), x_{t_s}, t_s) \cdot (t_{i+(k+1)} - t_i)$  holds, where the definition of the function  $h$  remains consistent with Sec. 3.1.*

The first assumption ensures the application of Taylor expansion in Eq. (15). The second assumption is based on the observation in Fig. 2a that when  $\Delta t$  is not excessively large, the MSE of the noise network remains almost unchanged across different time steps. The last one is based on the *Mean Value Theorem* for Integrals, which states that if  $f(x)$  is a continuous real-valued function on a closed interval  $[a, b]$ , then there exists at least one point  $c \in [a, b]$  such that  $\int_a^b f(x)dx = f(c)(b-a)$  holds.

**Remark 3.** *It is important to note that the Mean Value Theorem for Integrals originally applies to real-valued functions and does not directly apply to vector-valued functions [45]. However, the study by Zhou et al. [46], which uses Principal Component Analysis (PCA) on the trajectories of the ODE solvers for DPMs, demonstrates that these trajectories almost lie in a two-dimensional plane. The finding ensures the applicability of the Mean Value Theorem for Integrals in Assumption B.3.*

## B.2 Proof of Proposition 3.1

In this section, we prove that Eq. (16) holds, where  $\varepsilon \in (t_{i-1}, t_i)$  and  $n \geq 2$ . First, given  $\varepsilon \in (t_{i-1}, t_i)$ , we have:

$$|t_i - \varepsilon| + |t_{i-1} - \varepsilon| = |t_i - t_{i-1}|. \quad (\text{B.1})$$

Next, we analyze the Eq. (16) based on the parity of  $n$ .

**When  $n$  is even ( $n \geq 2$ ):** We derive:

$$\begin{aligned} \left| \frac{(t_i - \varepsilon)^n - (t_{i-1} - \varepsilon)^n}{n!} \right| &= \left| \frac{|t_i - \varepsilon|^n - |t_{i-1} - \varepsilon|^n}{n!} \right| \\ &< \max \left( \frac{|t_i - \varepsilon|^n}{n!}, \frac{|t_{i-1} - \varepsilon|^n}{n!} \right) \\ &< \frac{|t_i - t_{i-1}|^n}{n!} = \left| \frac{(t_i - t_{i-1})^n}{n!} \right|. \end{aligned} \quad (\text{B.2})$$

Here, the second “<” holds because: due to  $\varepsilon \in (t_{i-1}, t_i)$  and Eq. (B.1), we have  $|t_i - \varepsilon| < |t_i - t_{i-1}|$  and  $|t_{i-1} - \varepsilon| < |t_i - t_{i-1}|$ , thus validating the second “<”.

**When  $n$  is odd ( $n \geq 3$ ):** Since  $\varepsilon \in (t_{i-1}, t_i)$ , if  $t_i - \varepsilon > 0$ , then  $t_{i-1} - \varepsilon < 0$ ; if  $t_i - \varepsilon < 0$ , then  $t_{i-1} - \varepsilon > 0$ . Therefore, we obtain:

$$\left| \frac{(t_i - \varepsilon)^n - (t_{i-1} - \varepsilon)^n}{n!} \right| = \frac{|t_i - \varepsilon|^n + |t_{i-1} - \varepsilon|^n}{n!}. \quad (\text{B.3})$$

Let  $a = |t_i - \varepsilon|$ ,  $b = |t_{i-1} - \varepsilon|$ , and  $c = |t_i - t_{i-1}|$ ; we have  $a, b, c > 0$  and  $c > a, b$ . Next, using mathematical induction, we prove  $a^n + b^n < c^n$ , where  $n \geq 3$  and  $a + b = c$  (Eq. (B.1)).

- When  $n = 3$ , we have:

$$c^3 = (a + b)^3 = a^3 + 3a^2b + 3ab^2 + b^3 > a^3 + b^3, \quad (\text{B.4})$$

which holds.

- When  $n = k$  ( $k \geq 3, k \in \mathbb{N}$ ), suppose  $a \leq b$ , then  $a^k + b^k < c^k$  holds.
- When  $n = k + 1$ , we have:

$$a^{k+1} + b^{k+1} = a \cdot a^k + b \cdot b^k \leq b \cdot a^k + b \cdot b^k = b \cdot (a^k + b^k) < b \cdot c^k < c^{k+1}, \quad (\text{B.5})$$

which holds.

Thus,  $a^n + b^n < c^n$  holds, where  $n \geq 3$  and  $a + b = c$ . Furthermore, we obtain:

$$\frac{|t_i - \varepsilon|^n + |t_{i-1} - \varepsilon|^n}{n!} < \frac{|t_i - t_{i-1}|^n}{n!} = \left| \frac{(t_i - t_{i-1})^n}{n!} \right|. \quad (\text{B.6})$$

In conclusion, by combining Eq. (B.2), Eq. (B.3), and Eq. (B.6), we have proven Eq. (16).



### B.3 Proof of convergence for PFDiff

**Assumption B.2 ensures the convergence of PFDiff- $k\_h$  using past gradients.** Starting from Eq. (8), we consider an iteration process of a  $p$ -order ODE solver from  $\tilde{x}_{t_i}$  to  $\tilde{x}_{t_{i+h}}$ , where  $h$  is the “springboard” choice determined by PFDiff- $k\_h$ . This iterative process can be expressed as:

$$\tilde{x}_{t_{i+h}} = \tilde{x}_{t_i} + \int_{t_i}^{t_{i+h}} s(\epsilon_\theta(x_t, t), x_t, t) dt. \quad (\text{B.7})$$

Discretizing Eq. (B.7) yields:

$$\begin{aligned} \tilde{x}_{t_i \rightarrow t_{i+h}} &\approx \tilde{x}_{t_i} + \sum_{n=0}^{p-1} h(\epsilon_\theta(\tilde{x}_{\hat{t}_n}, \hat{t}_n), \tilde{x}_{\hat{t}_n}, \hat{t}_n) \cdot (\hat{t}_{n+1} - \hat{t}_n) \\ &= \tilde{x}_{t_i} + \sum_{n=i}^{i+h-1} h(\epsilon_\theta(\tilde{x}_{t_n}, t_n), \tilde{x}_{t_n}, t_n) \cdot (t_{n+1} - t_n), \end{aligned} \quad (\text{B.8})$$

where the function  $h$  represents the different solution methodologies applied by various  $p$ -order ODE solvers to the function  $s$ , consistent with Sec. 3.1. To accelerate sampler convergence and reduce unnecessary NFE, we adopt Assumption B.2, namely guiding the sampling of the current intermediate state by utilizing past gradient information. Specifically, we approximate that  $\left(\{\epsilon_\theta(\tilde{x}_{\hat{t}_n}, \hat{t}_n)\}_{n=0}^{p-1}, t_i, t_{i+h}\right) \approx \left(\{\epsilon_\theta(\tilde{x}_{\hat{t}_n}, \hat{t}_n)\}_{n=0}^{p-1}, t_{i-(k-h+1)}, t_i\right)$ , where  $k$  represents the number of steps skipped in one iteration by PFDiff- $k\_h$ . Eq. (B.8) can be further rewritten as:

$$\begin{aligned} \tilde{x}_{t_i \rightarrow t_{i+h}} &\approx \tilde{x}_{t_i} + \sum_{n=i-(k-h+1)}^{i-1} h(\epsilon_\theta(\tilde{x}_{t_n}, t_n), \tilde{x}_{t_n}, t_n) \cdot (t_{n+1} - t_n) \\ &= \phi\left(\left\{\epsilon_\theta(\tilde{x}_{\hat{t}_n}, \hat{t}_n)\right\}_{n=0}^{p-1}, t_{i-(k-h+1)}, t_i\right), \tilde{x}_{t_i}, t_i, t_{i+h}, \end{aligned} \quad (\text{B.9})$$

where  $\phi$  is any  $p$ -order ODE solver. Eq. (B.9) demonstrates that under Assumption B.2, PFDiff- $k\_h$  utilizes past gradients to replace current gradients, converging to the same data distribution as that of any  $p$ -order ODE solver  $\phi$ . However, as noted in Remark 2, the time step size  $\Delta t$  is very large (NFE<10), making “springboard”  $\tilde{x}_{t_{i+h}}$  unreliable in Eq. (B.9). Therefore, we only use  $\tilde{x}_{t_{i+h}}$  to predict a *foresight* update direction (i.e., the future gradient). The introduction of the future gradient can reduce the impact of neglecting higher-order derivative terms, thus correcting the discretization errors of the first-order ODE solvers.

**Convergence of PFDiff- $k\_h$  using future gradients.** As described in Sec. 3.3, higher-order ODE solvers and future gradients reduce the discretization error caused by neglecting higher-order derivative terms in two parallel manners. Therefore, PFDiff combines a higher-order ODE solver using only past gradients, with convergence guarantees based on Assumption B.2. Next, we consider an iteration process of a first-order ODE solver from  $\tilde{x}_{t_i}$  to  $\tilde{x}_{t_{i+(k+1)}}$ , which can be expressed as:

$$\begin{aligned} \tilde{x}_{t_{i+(k+1)}} &= \tilde{x}_{t_i} + \int_{t_i}^{t_{i+(k+1)}} s(\epsilon_\theta(x_t, t), x_t, t) dt \\ &\approx \tilde{x}_{t_i} + h(\epsilon_\theta(\tilde{x}_{t_i}, t_i), \tilde{x}_{t_i}, t_i) \cdot (t_{i+(k+1)} - t_i) \\ &= \phi(\epsilon_\theta(\tilde{x}_{t_i}, t_i), \tilde{x}_{t_i}, t_i, t_{i+(k+1)}), \end{aligned} \quad (\text{B.10})$$

where the second line is obtained by discretizing the first line with an existing first-order ODE solver, and the definitions of  $\phi$  and  $h$  are consistent with Sec. 3.1. It is well known that the “ $\approx$ ” in Eq. (B.10) introduces discretization errors. We have revised Eq. (B.10) based on Assumption B.3, as follows:

$$\begin{aligned} \tilde{x}_{t_{i+(k+1)}} &= \tilde{x}_{t_i} + \int_{t_i}^{t_{i+(k+1)}} s(\epsilon_\theta(x_t, t), x_t, t) dt \\ &= \tilde{x}_{t_i} + s(\epsilon_\theta(\tilde{x}_{t_{\bar{s}}}, t_{\bar{s}}), \tilde{x}_{t_{\bar{s}}}, t_{\bar{s}}) \cdot (t_{i+(k+1)} - t_i) \\ &= \tilde{x}_{t_i} + h(\epsilon_\theta(\tilde{x}_{t_s}, t_s), \tilde{x}_{t_s}, t_s) \cdot (t_{i+(k+1)} - t_i) \\ &= \phi(\epsilon_\theta(\tilde{x}_{t_s}, t_s), \tilde{x}_{t_i}, t_i, t_{i+(k+1)}). \end{aligned} \quad (\text{B.11})$$

Eq. (B.11) indicates that there is an optimal time point  $t_s \in [t_i, t_{i+(k+1)}]$  corresponding to the optimal gradient  $\epsilon_\theta(\tilde{x}_{t_s}, t_s)$  that can correct the discretization error of Eq. (B.10). Furthermore, when the time step size  $\Delta t = t_{i+(k+1)} - t_i$  is very large (for example, NFE<10), using the gradient at the current time point  $t_i$  leads to non-convergence of the sampling process. This implies that the sampling trajectory of DPMs is not a straight line (if it were a straight line, a larger sampling step size could be used). Therefore, the optimal time point is not achieved at the endpoints, i.e.,  $t_s \neq t_i$  and  $t_s \neq t_{i+(k+1)}$ , and we adjust that  $t_s$  falls within the interval  $(t_i, t_{i+(k+1)})$ . Additionally, to approximate the optimal gradient, we introduce the *foresight* update mechanism of the Nesterov momentum [35], and guide the current intermediate state sampling with future gradient information. In other words, we replace  $\epsilon_\theta(\tilde{x}_{t_s}, t_s)$  with  $\epsilon_\theta(\tilde{x}_{t_{i+h}}, t_{i+h})$ , as follows:

$$\begin{aligned}\tilde{x}_{t_{i+(k+1)}} &= \phi(\epsilon_\theta(\tilde{x}_{t_s}, t_s), \tilde{x}_{t_i}, t_i, t_{i+(k+1)}) \\ &\approx \phi(\epsilon_\theta(\tilde{x}_{t_{i+h}}, t_{i+h}), \tilde{x}_{t_i}, t_i, t_{i+(k+1)}),\end{aligned}\tag{B.12}$$

where  $k$  and  $h$  are determined by the selected PFDiff- $k_h$ . According to the definition of PFDiff- $k_h$ ,  $t_{i+h}$  also lies within the interval  $(t_i, t_{i+(k+1)})$ . For six different versions of PFDiff- $k_h$  defined in Appendix C, we believe the optimal  $t_s$  within the interval  $(t_i, t_{i+(k+1)})$  has been approximated, thereby completing the convergence proof of using future gradients. Finally, we note that PFDiff using future gradients to replace current gradients is an approximation of the optimal gradient. Together with this section and Proposition 3.1 (future gradients have less impact at neglecting higher-order derivative terms), we jointly verify that future gradients can more effectively guide a first-order ODE solver in sampling.

## C Algorithms of PFDiffs

As described in Sec. 3.4, during a single iteration, we can leverage the *foresight* update mechanism to skip to a more distant future. Specifically, we modify Eq. (14) to  $\tilde{x}_{t_{i+(k+1)}} \approx \phi(Q, \tilde{x}_{t_i}, t_i, t_{i+(k+1)})$  to achieve a  $k$ -step skip. We refer to this method as PFDiff- $k$ . Additionally, when  $k \neq 1$ , the computation of the buffer  $Q$ , originating from Eq. (13), presents different selection choices. We modify Eq. (12) to  $\tilde{x}_{t_{i+h}} \approx \phi(Q, \tilde{x}_{t_i}, t_i, t_{i+h})$ ,  $h \leq k$  to denote different “springboard” choices with the

---

### Algorithm 2 PFDiff-2

---

**Require:** initial value  $x_T$ , NFE  $N$ , model  $\epsilon_\theta$ , any  $p$ -order solver  $\phi$ , skip type  $h$

- 1: Define time steps  $\{t_i\}_{i=0}^M$  with  $M = 3N - 2p$
  - 2:  $\tilde{x}_{t_0} \leftarrow x_T$
  - 3:  $Q \leftarrow^{\text{buffer}} \left( \{\epsilon_\theta(\tilde{x}_{\hat{t}_n}, \hat{t}_n)\}_{n=0}^{p-1}, t_0, t_1 \right)$  ▷ Initialize buffer
  - 4:  $\tilde{x}_{t_1} = \phi(Q, \tilde{x}_{t_0}, t_0, t_1)$
  - 5: **for**  $i \leftarrow 1$  to  $\frac{M}{p} - 3$  **do**
  - 6:     **if**  $(i - 1) \bmod 3 = 0$  **then** ▷ PFDiff-2\_1
  - 7:         **if**  $h = 1$  **then** ▷ Updating guided by past gradients
  - 8:              $\tilde{x}_{t_{i+1}} = \phi(Q, \tilde{x}_{t_i}, t_i, t_{i+1})$
  - 9:              $Q \leftarrow^{\text{buffer}} \left( \{\epsilon_\theta(\tilde{x}_{\hat{t}_n}, \hat{t}_n)\}_{n=0}^{p-1}, t_{i+1}, t_{i+3} \right)$  ▷ Update buffer (overwrite)
  - 10:         **else if**  $h = 2$  **then** ▷ PFDiff-2\_2
  - 11:              $\tilde{x}_{t_{i+2}} = \phi(Q, \tilde{x}_{t_i}, t_i, t_{i+2})$  ▷ Updating guided by past gradients
  - 12:              $Q \leftarrow^{\text{buffer}} \left( \{\epsilon_\theta(\tilde{x}_{\hat{t}_n}, \hat{t}_n)\}_{n=0}^{p-1}, t_{i+2}, t_{i+3} \right)$  ▷ Update buffer (overwrite)
  - 13:         **end if**
  - 14:         **if**  $p = 1$  **then** ▷ Anticipatory updating guided by future gradients
  - 15:              $\tilde{x}_{t_{i+3}} = \phi(Q, \tilde{x}_{t_i}, t_i, t_{i+3})$
  - 16:         **else if**  $p > 1$  **then** ▷ The higher-order solver uses only past gradients
  - 17:              $\tilde{x}_{t_{i+3}} = \phi(Q, \tilde{x}_{t_{i+1}}, t_{i+1}, t_{i+3})$
  - 18:         **end if**
  - 19:     **end if**
  - 20: **end for**
  - 21: **return**  $\tilde{x}_{t_M}$
-

---

**Algorithm 3** PFDiff-3

---

**Require:** initial value  $x_T$ , NFE  $N$ , model  $\epsilon_\theta$ , any  $p$ -order solver  $\phi$ , skip type  $h$

- 1: Define time steps  $\{t_i\}_{i=0}^M$  with  $M = 4N - 3p$
- 2:  $\tilde{x}_{t_0} \leftarrow x_T$
- 3:  $Q \xleftarrow{\text{buffer}} \left( \{\epsilon_\theta(\tilde{x}_{\hat{t}_n}, \hat{t}_n)\}_{n=0}^{p-1}, t_0, t_1 \right)$  ▷ Initialize buffer
- 4:  $\tilde{x}_{t_1} = \phi(Q, \tilde{x}_{t_0}, t_0, t_1)$
- 5: **for**  $i \leftarrow 1$  to  $\frac{M}{p} - 4$  **do**
- 6:     **if**  $(i - 1) \bmod 4 = 0$  **then**
- 7:          $\tilde{x}_{t_{i+4}} = \phi(Q, \tilde{x}_{t_i}, t_i, t_{i+h})$  ▷ Updating guided by past gradients
- 8:          $Q \xleftarrow{\text{buffer}} \left( \{\epsilon_\theta(\tilde{x}_{\hat{t}_n}, \hat{t}_n)\}_{n=0}^{p-1}, t_{i+h}, t_{i+4} \right)$  ▷ Update buffer (overwrite)
- 9:         **if**  $p = 1$  **then**
- 10:              $\tilde{x}_{t_{i+4}} = \phi(Q, \tilde{x}_{t_i}, t_i, t_{i+4})$  ▷ Anticipatory updating guided by future gradients
- 11:         **else if**  $p > 1$  **then**
- 12:              $\tilde{x}_{t_{i+4}} = \phi(Q, \tilde{x}_{t_{i+h}}, t_{i+h}, t_{i+4})$  ▷ The higher-order solver uses only past gradients
- 13:         **end if**
- 14:     **end if**
- 15: **end for**
- 16: **return**  $\tilde{x}_{t_M}$

---

parameter  $h$ . This strategy of multi-step skips and varying “springboard” choices is collectively termed as PFDiff- $k_h$  ( $h \leq k$ ). Consequently, based on modifications to parameters  $k$  and  $h$  in Eq. (12) and Eq. (14), Eq. (13) is updated to  $Q \xleftarrow{\text{buffer}} \left( \{\epsilon_\theta(\tilde{x}_{\hat{t}_n}, \hat{t}_n)\}_{n=0}^{p-1}, t_{i+h}, t_{i+(k+1)} \right)$ , and Eq. (11) is updated to  $Q \xleftarrow{\text{buffer}} \left( \{\epsilon_\theta(\tilde{x}_{\hat{t}_n}, \hat{t}_n)\}_{n=0}^{p-1}, t_{i-(k-h+1)}, t_i \right)$ .

When  $k = 1$ , since  $h \leq k$ , then  $h = 1$ , and PFDiff- $k_h$  is the same as PFDiff-1, as shown in Algorithm 1 in Sec. 3.4. When  $k = 2$ ,  $h$  can be either 1 or 2, forming Algorithms PFDiff-2\_1 and PFDiff-2\_2, as shown in Algorithm 2. Furthermore, when  $k = 3$ , this forms three different versions of PFDiff-3, as shown in Algorithm 3. In this study, we utilize the optimal results from the six configurations of PFDiff- $k_h$  ( $k = 1, 2, 3$  ( $h \leq k$ )) to demonstrate the performance of PFDiff. As described in Appendix B.3, this is essentially an approximation of the optimal time point  $t_s$ . Through these six different algorithm configurations, we approximately search for the optimal  $t_s$ . It is important to note that despite using six different algorithm configurations, this does not increase the computational burden in practical applications. This is because, by visual analysis of a small number of generated images or computing specific evaluation metrics, one can effectively select

Table 1: The used datasets, codes, and their licenses.

Name	URL	License
CIFAR10 [42]	<a href="https://www.cs.toronto.edu/~kriz/cifar.html">https://www.cs.toronto.edu/~kriz/cifar.html</a>	\
CelebA 64x64 [43]	<a href="https://mmlab.ie.cuhk.edu.hk/projects/CelebA.html">https://mmlab.ie.cuhk.edu.hk/projects/CelebA.html</a>	\
LSUN-Bedroom [44]	<a href="https://www.yf.io/p/l_sun">https://www.yf.io/p/l_sun</a>	\
LSUN-Church [44]	<a href="https://www.yf.io/p/l_sun">https://www.yf.io/p/l_sun</a>	\
ImageNet [33]	<a href="https://image-net.org/">https://image-net.org/</a>	\
MS-COCO2014 [32]	<a href="https://cocodataset.org/">https://cocodataset.org/</a>	CC BY 4.0
ScoreSDE [4]	<a href="https://github.com/yang-song/score_sde_pytorch">https://github.com/yang-song/score_sde_pytorch</a>	Apache-2.0
DDIM [20]	<a href="https://github.com/ermongroup/ddim/tree/main">https://github.com/ermongroup/ddim/tree/main</a>	MIT
Analytic-DPM [23]	<a href="https://github.com/baoefff/Analytic-DPM">https://github.com/baoefff/Analytic-DPM</a>	\
DPM-Solver [21]	<a href="https://github.com/LuChengTHU/dpm-solver">https://github.com/LuChengTHU/dpm-solver</a>	MIT
DPM-Solver++ [22]	<a href="https://github.com/LuChengTHU/dpm-solver">https://github.com/LuChengTHU/dpm-solver</a>	MIT
Guided-Diffusion [5]	<a href="https://github.com/openai/guided-diffusion">https://github.com/openai/guided-diffusion</a>	MIT
Stable-Diffusion [9]	<a href="https://github.com/CompVis/stable-diffusion">https://github.com/CompVis/stable-diffusion</a>	CreativeML Open RAIL-M

the algorithm configuration with the best performance. Moreover, even without any selection, with  $k = 2$  and  $h = 1$  fixed, PFDiff-2\_1 can always improve the baseline’s sampling quality within the range of 4~20 NFEs, as shown in the ablation study results in Sec. 4.3.

## D Additional experiment results

In this section, we provide further supplements to the experiments on both unconditional and conditional pre-trained Diffusion Probabilistic Models (DPMs) as mentioned in Sec. 4. Through these additional supplementary experiments, we more fully validate the effectiveness of PFDiff as an orthogonal and training-free sampler. Unless otherwise stated, the selection of pre-trained DPMs, choice of baselines, algorithm configurations, GPU utilization, and other related aspects in this section are consistent with those described in Sec. 4.

Table 2: Sample quality measured by FID $\downarrow$  on the CIFAR10 [42], CelebA 64x64 [43], LSUN-bedroom 256x256 [44], and LSUN-church 256x256 [44] datasets using unconditional discrete-time DPMs, varying the number of function evaluations (NFE). Evaluated on 50k samples. PFDiff uses DDIM [20] and Analytic-DDIM [23] as baselines and introduces DDPM [2] and Analytic-DDPM [23] with  $\eta = 1.0$  from Eq. (6) for comparison.

+PFDiff	Method	NFE						
		4	6	8	10	12	15	20
CIFAR10 (discrete-time model [2], quadratic time steps)								
×	DDPM( $\eta = 1.0$ ) [2]	108.05	71.47	52.87	41.18	32.98	25.59	18.34
×	Analytic-DDPM [23]	65.81	56.37	44.09	34.95	29.96	23.26	17.32
×	Analytic-DDIM [23]	106.86	24.02	14.21	10.09	8.80	7.25	6.17
×	DDIM [20]	65.70	29.68	18.45	13.66	11.01	8.80	7.04
✓	Analytic-DDIM	289.84	23.24	7.03	<b>4.51</b>	<b>3.91</b>	<b>3.75</b>	<b>3.65</b>
✓	DDIM	<b>22.38</b>	<b>9.48</b>	<b>5.64</b>	4.57	4.39	4.10	3.68
CelebA 64x64 (discrete-time model [20], quadratic time steps)								
×	DDPM( $\eta = 1.0$ ) [2]	59.38	43.63	34.12	28.21	24.40	20.19	15.85
×	Analytic-DDPM [23]	32.10	39.78	32.29	26.96	23.03	19.36	15.67
×	Analytic-DDIM [23]	69.75	16.60	11.84	9.37	7.95	6.92	5.84
×	DDIM [20]	37.76	20.99	14.10	10.86	9.01	7.67	6.50
✓	Analytic-DDIM	360.21	28.24	5.66	4.90	4.62	<b>4.55</b>	<b>4.55</b>
✓	DDIM	<b>13.29</b>	<b>7.53</b>	<b>5.06</b>	<b>4.71</b>	<b>4.60</b>	4.70	4.68
CelebA 64x64 (discrete-time model [20], uniform time steps)								
×	DDPM( $\eta = 1.0$ ) [2]	65.39	49.52	41.65	36.68	33.45	30.27	26.76
×	Analytic-DDPM [23]	102.45	42.43	34.36	33.85	30.38	28.90	25.89
×	Analytic-DDIM [23]	90.44	24.85	16.45	16.67	15.11	15.00	13.40
×	DDIM [20]	<b>44.36</b>	29.12	23.19	20.50	18.43	16.71	14.76
✓	Analytic-DDIM	308.58	56.04	14.07	10.98	8.97	<b>6.39</b>	<b>5.19</b>
✓	DDIM	51.87	<b>12.79</b>	<b>8.82</b>	<b>8.93</b>	<b>7.70</b>	6.44	5.66
LSUN-bedroom 256x256 (discrete-time model [2], uniform time steps)								
×	DDIM [20]	<b>115.63</b>	47.40	26.73	19.26	15.23	11.68	9.26
✓	DDIM	140.40	<b>18.72</b>	<b>11.50</b>	<b>9.28</b>	<b>8.36</b>	<b>7.76</b>	<b>7.14</b>
LSUN-church 256x256 (discrete-time model [2], uniform time steps)								
×	DDIM [20]	121.95	50.02	30.04	22.04	17.66	14.58	12.49
✓	DDIM	<b>72.86</b>	<b>18.30</b>	<b>14.34</b>	<b>13.27</b>	<b>12.05</b>	<b>11.77</b>	<b>11.12</b>

## D.1 License

In this section, we list the used datasets, codes, and their licenses in Table 1.

## D.2 Additional results for unconditional discrete-time sampling

In this section, we report on experiments with unconditional, discrete DPMs on the CIFAR10 [42] and CelebA 64x64 [43] datasets using quadratic time steps. The  $\text{FID}\downarrow$  scores for the PFDiff algorithm are reported for changes in the number of function evaluations (NFE) from 4 to 20. Additionally, we present FID scores on the CelebA 64x64 [43], LSUN-bedroom 256x256 [44], and LSUN-church 256x256 [44] datasets, utilizing uniform time steps. The experimental results are summarized in Table 2. Results indicate that using DDIM [20] as the baseline, our method (PFDiff) nearly achieved significant performance improvements across all datasets and NFE settings. Notably, PFDiff facilitates rapid convergence of pre-trained DPMs to the data distribution with NFE settings below 10, validating its effectiveness on discrete pre-trained DPMs and the first-order ODE solver DDIM. It is important to note that on the CIFAR10 and CelebA 64x64 datasets, we have included the FID scores of Analytic-DDIM [23], which serves as another baseline. Analytic-DDIM modifies the variance in DDIM and introduces some random noise. With NFE lower than 10, the presence of minimal random noise amplifies the error introduced by the gradient information approximation in PFDiff, reducing its error correction capability compared to the Analytic-DDIM sampler. Thus, in fewer-step sampling ( $\text{NFE} < 10$ ), using DDIM as the baseline is more effective than using Analytic-DDIM, which requires recalculating the optimal variance for different pre-trained DPMs, thereby introducing additional computational overhead. In other experiments with pre-trained DPMs, we validate the efficacy of the PFDiff algorithm by combining it with the overall superior performance of the DDIM solver.

Table 3: Sample quality measured by  $\text{FID}\downarrow$  on the CIFAR10 [42] and CelebA 64x64 [43] using unconditional discrete-time DPMs with and without our method (PFDiff), varying the number of function evaluations (NFE) and  $\eta$  from Eq. (6). Evaluated on 50k samples.

Method	NFE						
	4	6	8	10	12	15	20
CIFAR10 (discrete-time model [2], quadratic time steps)							
DDPM( $\eta = 1.0$ ) [2]	108.05	71.47	52.87	41.18	32.98	25.59	18.34
+PFDiff (Ours)	475.47	432.24	344.96	332.41	285.88	158.90	28.05
DDPM( $\eta = 0.5$ ) [20]	71.08	34.32	22.37	16.63	13.37	10.75	8.38
+PFDiff (Ours)	432.50	349.09	311.62	167.65	59.93	23.17	10.61
DDPM( $\eta = 0.2$ ) [20]	66.33	30.26	18.94	14.01	11.25	9.00	7.18
+PFDiff (Ours)	316.15	189.02	18.55	7.73	5.70	4.53	4.00
DDIM( $\eta = 0.0$ ) [20]	65.70	29.68	18.45	13.66	11.01	8.80	7.04
+PFDiff (Ours)	<b>22.38</b>	<b>9.48</b>	<b>5.64</b>	<b>4.57</b>	<b>4.39</b>	<b>4.10</b>	<b>3.68</b>
CelebA 64x64 (discrete-time model [20], quadratic time steps)							
DDPM( $\eta = 1.0$ ) [2]	59.38	43.63	34.12	28.21	24.40	20.19	15.85
+PFDiff (Ours)	433.25	439.19	415.41	317.43	324.58	326.50	171.41
DDPM( $\eta = 0.5$ ) [20]	40.58	23.72	16.74	13.15	11.27	9.36	7.73
+PFDiff (Ours)	435.27	417.58	314.63	310.10	252.19	69.31	19.23
DDPM( $\eta = 0.2$ ) [20]	38.20	21.35	14.55	11.22	9.47	7.99	6.71
+PFDiff (Ours)	394.03	319.02	45.15	12.71	7.85	5.10	4.96
DDIM( $\eta = 0.0$ ) [20]	37.76	20.99	14.10	10.86	9.01	7.67	6.50
+PFDiff (Ours)	<b>13.29</b>	<b>7.53</b>	<b>5.06</b>	<b>4.71</b>	<b>4.60</b>	<b>4.70</b>	<b>4.68</b>

Furthermore, to validate the motivation proposed in Sec. 3.2 based on Fig. 2a—that at not excessively large time step size  $\Delta t$ , an ODE-based solver shows considerable similarity in the noise network outputs—we compare it with the SDE-based solver DDPM [2]. Even at smaller  $\Delta t$ , the mean squared error (MSE) of the noise outputs from DDPM remains high, suggesting that the effectiveness of PFDiff may be limited when based on SDE solvers. Further, we adjusted the  $\eta$  parameter in Eq. (6) (which controls the amount of noise introduced in DDPM) from 1.0 to 0.0 (at  $\eta = 0.0$ , the SDE-based DDPM degenerates into the ODE-based DDIM [20]). As shown in Fig. 2a, as  $\eta$  decreases, the MSE of the noise network outputs gradually decreases at the same time step size  $\Delta t$ , indicating that reducing noise introduction can enhance the effectiveness of PFDiff. To verify this motivation, we utilized quadratic time steps on CIFAR10 and CelebA 64x64 datasets and controlled the amount of noise introduced by adjusting  $\eta$ , to demonstrate that PFDiff can leverage the temporal redundancy present in ODE solvers to boost its performance. The experimental results, as shown in Table 3, illustrate that with the reduction of  $\eta$  from 1.0 (SDE) to 0.0 (ODE), PFDiff’s sampling performance significantly improves at fewer time steps ( $\text{NFE} \leq 20$ ). The experiment results regarding FID variations with NFE as presented in Table 3, align with the trends of MSE of noise network outputs with changes in time step size  $\Delta t$  as depicted in Fig. 2a. This reaffirms the motivation we proposed in Sec. 3.2.

### D.3 Additional results for unconditional continuous-time sampling

In this section, we supplement the specific  $\text{FID}\downarrow$  scores for the unconditional, continuous pre-trained DPMs models with first-order and higher-order ODE solvers, DPM-Solver-1, -2 and -3, [21] as baselines, as shown in Table 4. For all experiments in this section, we conducted tests on the CIFAR10 dataset [42], using the checkpoint `checkpoint_8.pth` under the `vp/cifar10_ddppmp_deep_continuous` configuration provided by ScoreSDE [4]. For the hyperparameter method of DPM-Solver [21], we adopted `singlestep_fixed`; to maintain consistency with the discrete-time model in Appendix D.2, the parameter `skip` was set to `time_quadratic` (i.e., quadratic time steps). Unless otherwise specified, we used the parameter settings recommended by DPM-Solver. The results in Table 4 show that by using the PFDiff method described in Sec. 3.4 and taking DPM-Solver as the baseline, we were able to further enhance sampling performance on the basis of first-order and higher-order ODE solvers. Particularly, in the 6~12 NFE range, PFDiff significantly improved the convergence issues of higher-order ODE solvers under fewer NFEs. For instance, at 9 NFE, PFDiff reduced the FID of DPM-Solver-3 from 233.56 to 5.67, improving the sampling quality by 97.57%. These results validate the effectiveness of using PFDiff with first-order or higher-order ODE solvers as the baseline.

Table 4: Sample quality measured by  $\text{FID}\downarrow$  of different orders of DPM-Solver [21] on the CIFAR10 [42] using unconditional continuous-time DPMs with and without our method (PFDiff), varying the number of function evaluations (NFE). Evaluated on 50k samples.

Method	order	NFE						
		4	6	8	10	12	16	20
CIFAR10 (continuous-time model [4], quadratic time steps)								
DPM-Solver-1 [21]	1	<b>40.55</b>	23.86	15.57	11.64	9.64	7.23	6.06
+PFDiff (Ours)	1	113.74	<b>11.41</b>	<b>5.90</b>	<b>4.23</b>	<b>3.92</b>	<b>3.73</b>	<b>3.75</b>
DPM-Solver-2 [21]	2	298.79	106.05	41.79	14.43	6.75	<b>4.24</b>	<b>3.91</b>
+PFDiff (Ours)	2	<b>85.22</b>	<b>16.30</b>	<b>9.67</b>	<b>6.64</b>	<b>5.74</b>	5.12	4.78
			6	9	12	15	21	
DPM-Solver-3 [21]	3		382.51	233.56	44.82	7.98	<b>3.63</b>	
+PFDiff (Ours)	3		<b>103.22</b>	<b>5.67</b>	<b>5.72</b>	<b>5.62</b>	5.24	



Table 5: Sample quality measured by FID $\downarrow$  on the ImageNet 64x64 [33] and ImageNet 256x256 [33], using ADM-G [5] model with guidance scales of 1.0 and 2.0, varying the number of function evaluations (NFE). Evaluated: ImageNet 64x64 with 50k, ImageNet 256x256 with 10k samples. \*We directly borrowed the results reported by AutoDiffusion [26], and AutoDiffusion requires additional search costs. \*We directly borrowed the results reported by AutoDiffusion [26], and AutoDiffusion requires additional search costs. “\” represents missing data in the original paper.

Method	Step	NFE					
		4	6	8	10	15	20
ImageNet 64x64 (pixel DPMs model [5], uniform time steps, guidance scale 1.0)							
DDIM [20]	Single	138.81	23.58	12.54	8.93	5.52	4.45
DPM-Solver-2 [21]	Single	327.09	292.66	264.97	236.80	166.52	120.29
DPM-Solver-2 [21]	Multi	48.64	21.08	12.45	8.86	5.57	4.46
DPM-Solver-3 [21]	Single	383.71	376.86	380.51	378.32	339.34	280.12
DPM-Solver-3 [21]	Multi	54.01	24.76	13.17	8.85	5.48	4.41
DPM-Solver++(2M) [22]	Multi	44.15	20.44	12.53	8.95	5.53	4.33
*AutoDiffusion [26]	Single	17.86	11.17	\	6.24	4.92	3.93
DDIM+PFDiff (Ours)	Single	<b>16.46</b>	<b>8.20</b>	<b>6.22</b>	<b>5.19</b>	<b>4.20</b>	<b>3.83</b>
ImageNet 256x256 (pixel DPMs model [5], uniform time steps, guidance scale 2.0)							
DDIM [20]	Single	51.79	23.48	16.33	12.93	9.89	9.05
DDIM+PFDiff (Ours)	Single	<b>37.81</b>	<b>18.15</b>	<b>12.22</b>	<b>10.33</b>	<b>8.59</b>	<b>8.08</b>

#### D.4 Additional results for classifier guidance

In this section, we provide the specific FID scores for pre-trained DPMs in the conditional, classifier guidance paradigm on the ImageNet 64x64 [33] and ImageNet 256x256 datasets [33], as shown in Table 5. We now describe the experimental setup in detail. For the pre-trained models, we used the ADM-G [5] provided `64x64_diffusion.pt` and `64x64_classifier.pt` for the ImageNet 64x64 dataset, and `256x256_diffusion.pt` and `256x256_classifier.pt` for the ImageNet 256x256 dataset. All experiments were conducted with uniform time steps and used DDIM as the baseline [20]. We implemented the second-order and third-order methods from DPM-Solver [21] for comparison and explored the method hyperparameter provided by DPM-Solver for both `singlestep` (corresponding to “Single” in Table 5) and `multistep` (corresponding to “Multi” in Table 5). Additionally, we implemented the best-performing method from DPM-Solver++ [22], multi-step DPM-Solver++(2M), as a comparative measure. Furthermore, we also introduced the superior-performing AutoDiffusion [26] method as a comparison. \*We directly borrowed the results reported in the original paper, emphasizing that although AutoDiffusion does not require additional training, it incurs additional search costs. “\” represents missing data in the original paper. The specific experimental results of the configurations mentioned are shown in Table 5. The results demonstrate that PFDiff, using DDIM as the baseline on the ImageNet 64x64 dataset, significantly enhances the sampling efficiency of DDIM and surpasses previous optimal training-free sampling methods. Particularly, in cases where  $NFE \leq 10$ , PFDiff improved the sampling quality of DDIM by 41.88%~88.14%. Moreover, on the large ImageNet 256x256 dataset, PFDiff demonstrates a consistent performance improvement over the DDIM baseline, similar to the improvements observed on the ImageNet 64x64 dataset.

#### D.5 Additional results for classifier-free guidance

In this section, we supplemented the specific FID $\downarrow$  scores for the Stable-Diffusion [9] (conditional, classifier-free guidance paradigm) setting with a guidance scale ( $s$ ) of 7.5 and 1.5. Specifically, for the pre-trained model, we conducted experiments using the `sd-v1-4.ckpt` checkpoint provided by Stable-Diffusion. All experiments used the MS-COCO2014 [32] validation set to calculate FID $\downarrow$  scores, with uniform time steps. PFDiff employs the DDIM [20] method as the baseline. Initially, under the recommended  $s = 7.5$  configuration by Stable-Diffusion, we implemented DPM-Solver-2

Table 6: Sample quality measured by FID $\downarrow$  on the validation set of MS-COCO2014 [32] using Stable-Diffusion model [9] with guidance scales of 7.5 and 1.5, varying the number of function evaluations (NFE). Evaluated on 10k samples.  $\dagger$ We borrow the results reported in DPM-Solver-v3 [27] directly.

Method	Step	NFE					
		5	6	8	10	15	20
MS-COCO2014 (latent DPMs model [9], uniform time steps, guidance scale 7.5)							
DDIM [20]	Single	23.92	20.33	17.46	16.78	16.08	15.95
DPM-Solver-2 [21]	Single	84.15	74.02	31.87	17.63	15.15	13.77
DPM-Solver-2 [21]	Multi	18.97	17.37	16.29	15.99	14.32	14.38
DPM-Solver-3 [21]	Single	156.27	102.59	54.52	26.29	16.95	14.85
DPM-Solver-3 [21]	Multi	18.89	17.34	16.25	16.11	14.10	<b>13.44</b>
$\dagger$ DPM-Solver++(2M) [22]	Multi	18.87	17.44	16.40	15.93	15.84	15.72
$\dagger$ UniPC [30]	Multi	18.77	17.32	16.20	16.15	16.06	15.94
$\dagger$ DPM-Solver-v3(2M) [27]	Multi	18.83	16.41	15.41	15.32	15.30	15.23
DDIM+PFDiff (Ours)	Single	<b>18.31</b>	<b>15.47</b>	<b>13.26</b>	<b>13.06</b>	<b>13.57</b>	13.97
MS-COCO2014 (latent DPMs model [9], uniform time steps, guidance scale 1.5)							
DDIM [20]	Single	70.36	54.32	37.54	29.41	20.54	18.17
DPM-Solver-2 [21]	Multi	37.47	27.79	19.65	18.39	17.27	16.85
DPM-Solver-3 [21]	Multi	35.90	25.88	18.26	19.10	17.21	16.67
DPM-Solver++(2M) [22]	Multi	36.58	26.78	18.92	20.26	18.61	17.78
DDIM+PFDiff (Ours)	Single	<b>24.31</b>	<b>20.99</b>	<b>18.09</b>	<b>17.00</b>	<b>16.03</b>	<b>15.57</b>

and -3 as comparative methods, and conducted searches for the method hyperparameters provided by DPM-Solver as `singlestep` (corresponding to “Single” in Table 6) and `multistep` (corresponding to “Multi” in Table 6). Additionally, we introduced previous state-of-the-art training-free methods, including DPM-Solver++(2M) [22], UniPC [30], and DPM-Solver-v3(2M) [27] for comparison. The experimental results are shown in Table 6.  $\dagger$ We borrow the results reported in DPM-Solver-v3 [27] directly. The results indicate that on Stable-Diffusion, PFDiff, using only DDIM as a baseline, surpasses the previous state-of-the-art training-free sampling methods in terms of sampling quality in fewer steps (NFE<20). Particularly, at NFE=10, PFDiff achieved a 13.06 FID, nearly converging to the data distribution, which is a 14.25% improvement over the previous state-of-the-art method DPM-Solver-v3 at 20 NFE, which had a 15.23 FID. Furthermore, to further validate the effectiveness of PFDiff on Stable-Diffusion, we conducted experiments using the  $s = 1.5$  setting with the same experimental configuration as  $s = 7.5$ . For the comparative methods, we only experimented with the multi-step versions of DPM-Solver-2 and -3 and DPM-Solver++(2M), which had faster convergence at fewer NFE under the  $s = 7.5$  setting. As for UniPC and DPM-Solver-v3(2M), since DPM-Solver-v3 did not provide corresponding experimental results at  $s = 1.5$ , we did not list their comparative results. The experimental results show that PFDiff, using DDIM as the baseline under the  $s = 1.5$  setting, demonstrated consistent performance improvements as seen in the  $s = 7.5$  setting, as shown in Table 6.

## D.6 Additional ablation study results

### D.6.1 Additional results for PFDiff hyperparameters study

In this section, we extensively investigate the impact of the hyperparameters  $k$  and  $h$  on the performance of the PFDiff algorithm, supplementing with the results of ablation experiments and experimental setups. Specifically, for the unconditional DPMs, we conducted experiments on the CIFAR10 dataset [42] using quadratic time steps, based on pre-trained unconditional discrete DDPM [2]. For the conditional DPMs, we used uniform time steps in classifier guidance ADM-G [5] pre-trained DPMs, setting the guidance scale ( $s$ ) to 1.0 for experiments on the ImageNet 64x64 dataset [33]. All experiments were conducted using the DDIM [20] algorithm as a baseline, and PFDiff- $k_h$  con-

Table 7: Ablation study of the impact of  $k$  and  $h$  on PFDiff in CIFAR10 [42] and ImageNet 64x64 [33] datasets using DDPM [2] and ADM-G [5] models. We report the FID $\downarrow$ , varying the number of function evaluations (NFE) and the number of samples for evaluating algorithm performance.

Samples	Method	NFE						
		4	6	8	10	12	15	20
CIFAR10 (unconditional DPMs model [2], quadratic time steps)								
50k	DDIM [20]	65.70	29.68	18.45	13.66	11.01	8.80	7.04
	+PFDiff-1	124.73	19.45	5.78	4.95	4.63	4.25	4.14
	+PFDiff-2_1	59.61	<b>9.84</b>	7.01	6.31	5.58	5.18	4.78
	+PFDiff-2_2	167.12	53.22	8.43	4.95	4.41	<b>4.10</b>	3.78
	+PFDiff-3_1	<b>22.38</b>	13.40	9.40	7.70	6.73	6.03	5.05
	+PFDiff-3_2	129.18	19.35	<b>5.64</b>	<b>4.57</b>	<b>4.39</b>	4.19	4.08
	+PFDiff-3_3	205.87	76.62	20.84	5.71	4.73	4.41	<b>3.68</b>
5k	DDIM[20]	69.79	34.20	22.84	17.39	15.56	12.87	11.62
	+PFDiff-1	127.82	23.96	10.35	9.73	9.29	9.09	8.74
	+PFDiff-2_1	63.59	<b>14.34</b>	11.40	11.08	9.23	10.03	9.38
	+PFDiff-2_2	170.58	57.74	12.94	9.86	10.08	<b>9.02</b>	8.44
	+PFDiff-3_1	<b>26.85</b>	17.93	13.95	12.37	9.59	10.89	9.65
	+PFDiff-3_2	132.45	23.80	<b>10.11</b>	<b>9.58</b>	<b>9.16</b>	9.09	8.69
	+PFDiff-3_3	208.80	80.13	24.84	10.73	11.16	9.14	<b>8.34</b>
ImageNet 64x64 (conditional DPMs model [5], uniform time steps, $s = 1.0$ )								
50k	DDIM [20]	138.81	23.58	12.54	8.93	6.74	5.52	4.45
	+PFDiff-1	26.86	11.39	7.47	5.83	5.16	4.76	4.39
	+PFDiff-2_1	17.14	8.94	6.38	5.46	5.46	4.30	<b>3.83</b>
	+PFDiff-2_2	23.66	9.93	6.86	5.72	5.17	4.49	3.94
	+PFDiff-3_1	16.74	9.43	7.19	5.86	5.07	4.69	4.44
	+PFDiff-3_2	<b>16.46</b>	<b>8.20</b>	<b>6.22</b>	<b>5.19</b>	<b>4.62</b>	<b>4.20</b>	4.28
	+PFDiff-3_3	23.06	9.73	6.92	5.55	5.21	4.47	4.49
5k	DDIM[20]	146.03	29.61	19.11	15.13	13.15	11.65	10.81
	+PFDiff-1	32.82	17.80	13.61	12.16	11.20	10.99	10.82
	+PFDiff-2_1	23.70	14.81	12.38	11.82	11.53	10.77	<b>10.24</b>
	+PFDiff-2_2	30.10	16.35	13.09	11.80	11.68	10.67	10.56
	+PFDiff-3_1	23.09	15.78	13.21	12.09	11.71	11.00	10.77
	+PFDiff-3_2	<b>22.54</b>	<b>14.23</b>	<b>12.24</b>	<b>11.27</b>	<b>11.16</b>	<b>10.47</b>	10.48
	+PFDiff-3_3	29.45	16.12	13.25	11.90	11.29	10.68	10.66

figurations ( $k = 1, 2, 3$  ( $h \leq k$ )) were tested in six different algorithm configurations. The FID $\downarrow$  scores are presented in Table 7, by varying the number of function evaluations (NFE) and the sample number used to compute the evaluation metrics.

We first analyze the impact of the hyperparameters  $k$  and  $h$  using 50k samples to compute the FID scores, which is a common method for evaluating the performance of sampling algorithms. The experimental results demonstrate that, under various combinations of  $k$  and  $h$ , PFDiff is able to enhance the sampling performance of the DDIM baseline in most cases across different types of pre-trained DPMs. Particularly when setting  $k = 2$  and  $h = 1$ , PFDiff-2\_1 can always improve the sampling performance of the DDIM baseline within the range of 4~20 NFE. Furthermore, we have an exciting discovery regarding the further optimization of algorithm performance: Searching with just 1/10 of the data provides consistent results compared to searches using the full 50k samples, significantly reducing the cost of hyperparameter searching for  $k$  and  $h$ . Specifically, for the same NFE, the optimal combinations of  $k$  and  $h$  based on FID scores are consistent for both 5k and 50k samples. For instance, when NFE=6, the best FID values for both 5k and 50k samples are achieved with  $k = 2$  and  $h = 1$ . For the six combinations used in this study with  $k \leq 3$  ( $h \leq k$ ), only a total of 30k samples are required to search the optimal  $k$  and  $h$  combination for each NFE—this is even

Table 8: Ablation study of the impact of the past and future gradients on PFDiff, using DDIM [20] as the baseline, in CIFAR10 [42] and CelebA 64x64 [43] datasets using discrete-time models [2, 20]. We report the FID $\downarrow$ , varying the number of function evaluations (NFE). Evaluated on 50k samples.

+PFDiff	Method	NFE						
		4	6	8	10	12	16	20
CIFAR10 (discrete-time model [2], quadratic time steps)								
×	DDIM [20]	65.70	29.68	18.45	13.66	11.01	8.80	7.04
×	+Cache [28]	49.02	24.04	15.23	11.31	9.40	7.25	6.25
×	+Past	52.81	27.47	17.87	13.64	10.79	8.20	7.02
×	+Future	66.06	25.39	11.93	8.06	6.04	4.17	4.07
✓	+Past & Future	<b>22.38</b>	<b>9.84</b>	<b>5.64</b>	<b>4.57</b>	<b>4.39</b>	<b>4.10</b>	<b>3.68</b>
CelebA 64x64 (discrete-time model [20], uniform time steps)								
×	DDIM [20]	44.36	29.12	23.19	20.50	18.43	16.13	14.76
×	+Cache [28]	33.86	25.95	22.29	19.83	18.28	16.05	14.45
×	+Past	<b>28.45</b>	21.56	18.65	17.03	15.89	14.05	12.73
×	+Future	39.85	16.30	14.40	12.79	12.13	9.73	8.13
✓	+Past & Future	51.87	<b>12.79</b>	<b>8.82</b>	<b>8.93</b>	<b>7.70</b>	<b>6.44</b>	<b>5.66</b>

less than the cost of evaluating algorithm performance normally with 50k samples. Additionally, in practical applications where only a small number of samples are needed for visual analysis, we can minimize training resources and rapidly identify the optimal  $k$  and  $h$  combination. In summary, the hyperparameters  $k$  and  $h$  do not impede the practical application of PFDiff in accelerating the sampling of DPMs.

Table 9: Inference time $\downarrow$  (second, mean $\pm$ std) required per 1k samples on a single NVIDIA 3090 GPU, varying the number of function evaluations (NFE). We additionally present the inference time with only past or only future gradients, at the same NFE. Moreover, we introduce methods [28, 29] that cache part of past gradients for comparison.

+PFDiff	Method	NFE			
		4	10	16	20
CIFAR10 (discrete-time model [2], quadratic time steps)					
×	DDIM [20]	6.14 $\pm$ 0.010	9.81 $\pm$ 0.022	13.58 $\pm$ 0.090	15.90 $\pm$ 0.081
×	+Cache [28]	6.31 $\pm$ 0.150	13.55 $\pm$ 0.019	19.42 $\pm$ 0.091	24.07 $\pm$ 0.185
×	+Past	6.17 $\pm$ 0.029	9.88 $\pm$ 0.040	13.66 $\pm$ 0.257	15.81 $\pm$ 0.062
×	+Future	6.16 $\pm$ 0.036	9.77 $\pm$ 0.153	13.73 $\pm$ 0.345	15.67 $\pm$ 0.096
✓	+Past & Future	6.10 $\pm$ 0.006	9.74 $\pm$ 0.036	13.48 $\pm$ 0.220	15.79 $\pm$ 0.036
CelebA 64x64 (discrete-time model [20], uniform time steps)					
×	DDIM [20]	13.65 $\pm$ 0.116	27.29 $\pm$ 0.543	40.55 $\pm$ 0.618	49.43 $\pm$ 0.497
×	+Cache [28]	19.82 $\pm$ 0.130	45.60 $\pm$ 0.131	71.70 $\pm$ 0.266	89.45 $\pm$ 0.085
×	+Past	13.67 $\pm$ 0.057	26.88 $\pm$ 0.144	40.24 $\pm$ 0.151	49.82 $\pm$ 0.081
×	+Future	13.61 $\pm$ 0.304	26.38 $\pm$ 0.067	39.95 $\pm$ 0.440	49.05 $\pm$ 0.543
✓	+Past & Future	13.21 $\pm$ 0.060	26.41 $\pm$ 0.042	40.26 $\pm$ 0.186	49.38 $\pm$ 0.257

### D.6.2 Ablation study of gradient guidance

To further investigate the impact of gradient guidance from the past or future on first-order ODE solvers on the rapid updating of current intermediate states, this section supplements related ablation study results and their settings. Specifically, we first use PFDiff with the first-order ODE solver DDIM [20] as a baseline, removing past and future gradients separately based on the discrete-time pre-trained models [2, 20]. On the CIFAR10 [42] and CelebA 64x64 [43] datasets, we alter the number of function evaluations (NFE) to compute the FID $\downarrow$  metric. Additionally, we introduce a method from previous literature [28] that accelerates sampling by caching part of past gradients for comparison. Specifically, we configure the hyperparameters based on the DeepCache [28] codebase, setting `cache_interval` to 2 and `branch` to 0, with all other settings remaining unchanged. As shown in Table 8, the experimental results indicate that using only past gradients or only future gradients can slightly improve the first-order ODE solvers sampling performance. However, their combined use (i.e., the complete PFDiff) significantly enhances first-order ODE solvers sampling performance, especially with very few steps (NFE<10), a phenomenon particularly evident. These results further validate the efficiency of the PFDiff algorithm when NFE<10, benefiting from its information-efficient update process, which utilizes past and future (complementing each other) gradients to jointly guide the current intermediate state.

Table 10: Sample quality measured by IS $\uparrow$  on the CIFAR10 [42], ImageNet 64x64 [33] and ImageNet 256x256 [33] using DDPM [2], ScoreSDE [4] and ADM-G [5] models, varying the number of function evaluations (NFE). Evaluated: ImageNet 256x256 with 10k, others with 50k samples. \*We directly borrowed the results reported by AutoDiffusion [26], and AutoDiffusion requires additional search costs. “\” represents missing data in the original paper and DPM-Solver-2 [21] implementation.

+PFDiff	Method	NFE					
		4	6	8	10	15	20
CIFAR10 (discrete-time model [2], quadratic time steps)							
×	DDPM( $\eta = 1.0$ ) [2]	4.32	5.66	6.55	7.08	7.91	8.25
×	Analytic-DDPM [23]	5.76	6.29	6.93	7.42	8.07	8.33
×	Analytic-DDIM [23]	4.46	7.47	8.11	8.43	8.72	8.89
×	DDIM [20]	5.68	7.21	7.92	8.26	8.62	8.81
✓	Analytic-DDIM	1.62	8.78	9.43	<b>9.61</b>	<b>9.35</b>	<b>9.29</b>
✓	DDIM	<b>7.79</b>	<b>9.29</b>	<b>9.62</b>	9.43	9.29	<b>9.29</b>
CIFAR10 (continuous-time model [4], quadratic time steps)							
×	DPM-Solver-1 [21]	<b>7.20</b>	8.30	8.85	8.98	9.43	9.51
×	DPM-Solver-2 [21]	1.70	5.29	7.94	9.09	\	9.74
✓	DPM-Solver-1	4.29	<b>9.25</b>	<b>9.76</b>	<b>9.86</b>	<b>9.85</b>	<b>9.97</b>
✓	DPM-Solver-2	6.96	8.58	8.75	9.26	\	9.69
ImageNet 64x64 (pixel DPMs model [5], uniform time steps, guidance scale 1.0)							
×	DDIM [20]	7.02	31.13	40.51	46.06	54.37	59.09
×	DPM-Solver-2(Multi) [21]	19.03	33.75	44.65	51.79	62.18	67.69
×	DPM-Solver-3(Multi) [21]	17.46	29.80	41.86	50.90	62.68	68.44
×	DPM-Solver++(2M) [22]	20.72	34.22	43.62	50.02	60.00	65.66
×	*AutoDiffusion [26]	34.88	43.37	\	57.85	64.03	68.05
✓	DDIM	<b>35.67</b>	<b>50.14</b>	<b>58.42</b>	<b>59.78</b>	<b>64.54</b>	<b>69.09</b>
ImageNet 256x256 (pixel DPMs model [5], uniform time steps, guidance scale 2.0)							
×	DDIM [20]	37.72	95.90	122.13	144.13	165.91	179.27
✓	DDIM	<b>55.90</b>	<b>122.56</b>	<b>158.57</b>	<b>169.72</b>	<b>183.07</b>	<b>192.70</b>

Furthermore, to verify whether the update process of the PFDiff algorithm increases additional inference time, we employed the same experimental settings as in Table 8 and provided a specific inference time comparison under different NFE. The inference time $\downarrow$  (second, mean $\pm$ std) required per 1k samples on a single NVIDIA 3090 GPU is shown in Table 9. The experimental results reveal that PFDiff+DDIM has consistent inference times with DDIM alone under the same NFE, indicating that the PFDiff algorithm does not add extra inference time. Additionally, methods [28] that cache part of past gradients not only incur additional inference costs but also exhibit relatively weak acceleration effects with a small number of steps (NFE $<$ 10). These results collectively demonstrate that the PFDiff algorithm can significantly enhance sampling quality without any increase in inference time, further proving its effectiveness.

### D.7 Inception score experimental results

To evaluate the effectiveness of the PFDiff algorithm and the widely used Fréchet Inception Distance (FID $\downarrow$ ) metric [40] in the sampling process of Diffusion Probabilistic Models (DPMs), we have also incorporated the Inception Score (IS $\uparrow$ ) metric [41] for both unconditional and conditional pre-trained DPMs. Specifically, for the unconditional discrete-time pre-trained DPMs DDPM [2], we maintained the experimental configurations described in Table 2 of Appendix D.2, and added IS scores for the CIFAR10 dataset [42]. For the unconditional continuous-time pre-trained DPMs ScoreSDE[4], the experimental configurations are consistent with Table 4 in Appendix D.3, and IS scores for the CIFAR10 dataset were also added. For the conditional classifier guidance paradigm of pre-trained DPMs ADM-G [5], the experimental setup aligned with Table 5 in Appendix D.4, including IS scores for the ImageNet 64x64 and ImageNet 256x256 datasets [33]. Considering that the computation of IS scores relies on features extracted using `InceptionV3` pre-trained on the ImageNet dataset, calculating IS scores for non-ImageNet datasets was not feasible, hence no IS scores were provided for the classifier-free guidance paradigm of Stable-Diffusion [9]. The experimental results are presented in Table 10. A comparison between the FID $\downarrow$  metrics in Tables 2, 4, and 5 and the IS $\uparrow$  metrics in Table 10 shows that both IS and FID metrics exhibit similar trends under the same experimental settings, i.e., as the number of function evaluations (NFE) changes, lower FID scores correspond to higher IS scores. Further, Figs. 1a and 1b, along with the visualization experiments in Appendix D.8, demonstrate that lower FID scores and higher IS scores correlate with higher image quality and richer details generated by the PFDiff sampling algorithm. These results further confirm the effectiveness of the PFDiff algorithm and the FID metric in evaluating the performance of sampling algorithms.

### D.8 Additional visualize study results

To demonstrate the effectiveness of PFDiff, we present the visual sampling results on the CIFAR10 [42], CelebA 64x64 [43], LSUN-bedroom 256x256 [44], LSUN-church 256x256 [44], ImageNet 64x64 [33], ImageNet 256x256 [33], and MS-COCO2014 [32] datasets in Figs. 6-11. These results illustrate that PFDiff, using different orders of ODE solvers as a baseline, is capable of generating samples of higher quality and richer detail on both unconditional and conditional pre-trained Diffusion Probabilistic Models (DPMs).



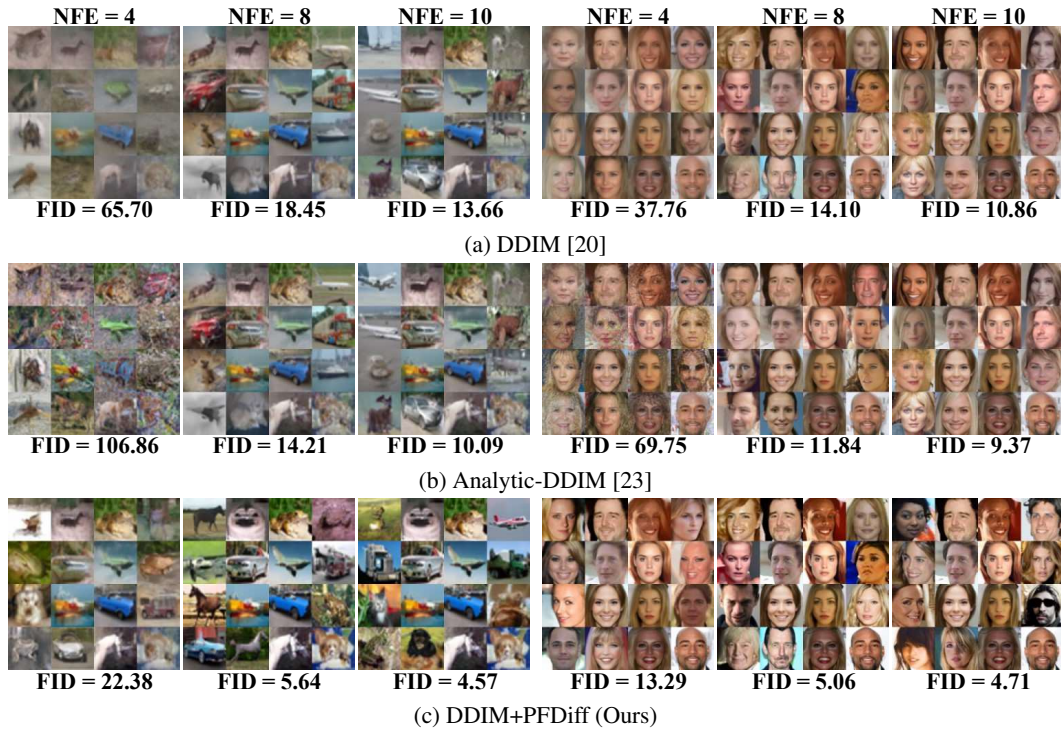


Figure 6: Random samples by DDIM [20], Analytic-DDIM [23], and PFDiff (baseline: DDIM) with 4, 8, and 10 number of function evaluations (NFE), using the same random seed, quadratic time steps, and pre-trained discrete-time DPMs [2, 20] on CIFAR10 [42] (left) and CelebA 64x64 [43] (right).



Figure 7: Random samples by DDIM [20] and PFDiff (baseline: DDIM) with 5 and 10 number of function evaluations (NFE), using the same random seed, uniform time steps, and pre-trained discrete-time DPMs [2] on LSUN-bedroom 256x256 [44] (left) and LSUN-church 256x256 [44] (right).

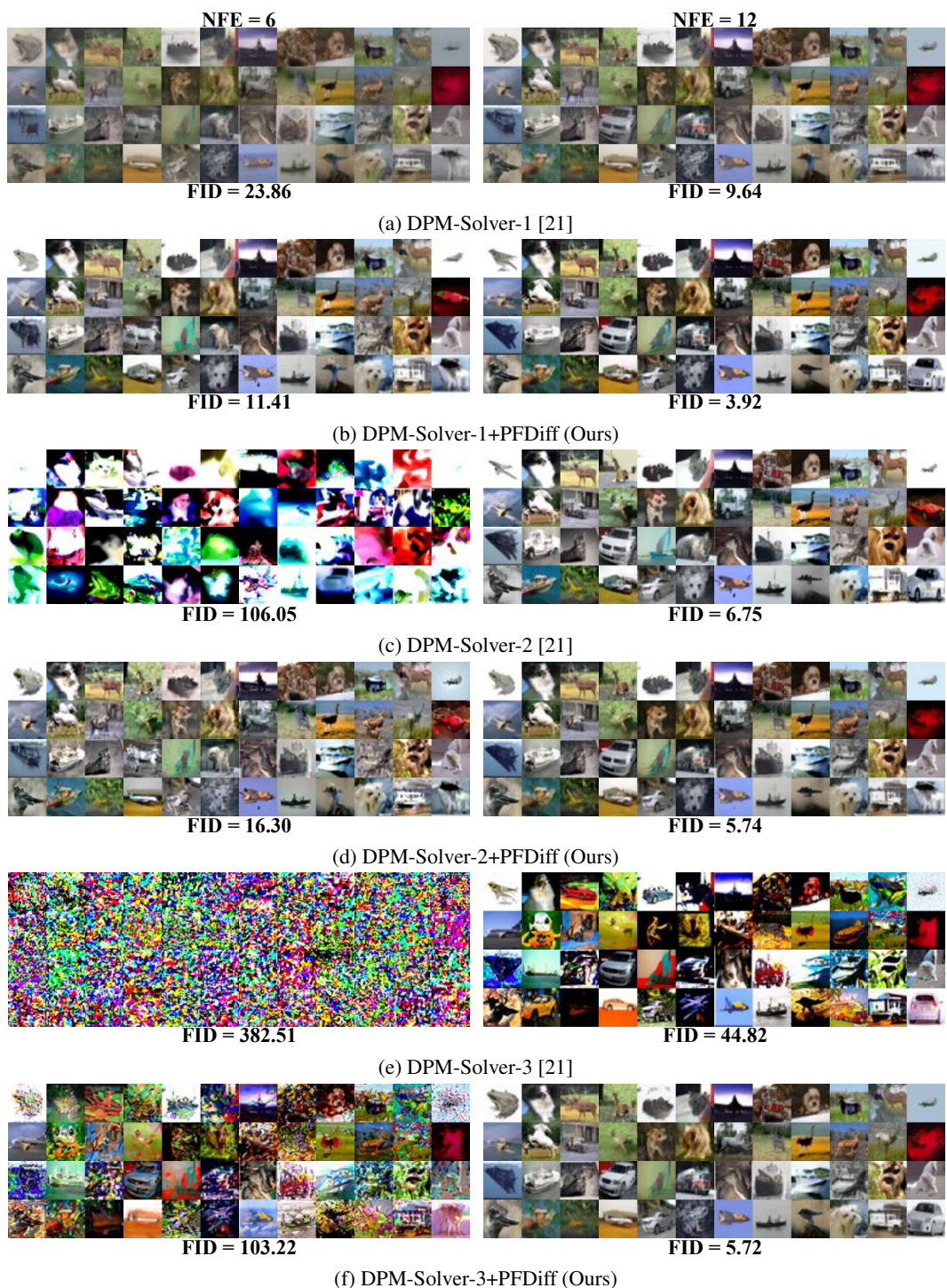


Figure 8: Random samples by DPM-Solver-1, -2, and -3 [21] with and without our method (PFDiff) with 6 and 12 number of function evaluations (NFE), using the same random seed, quadratic time steps, and pre-trained continuous-time DPMs [4] on CIFAR10 [42].



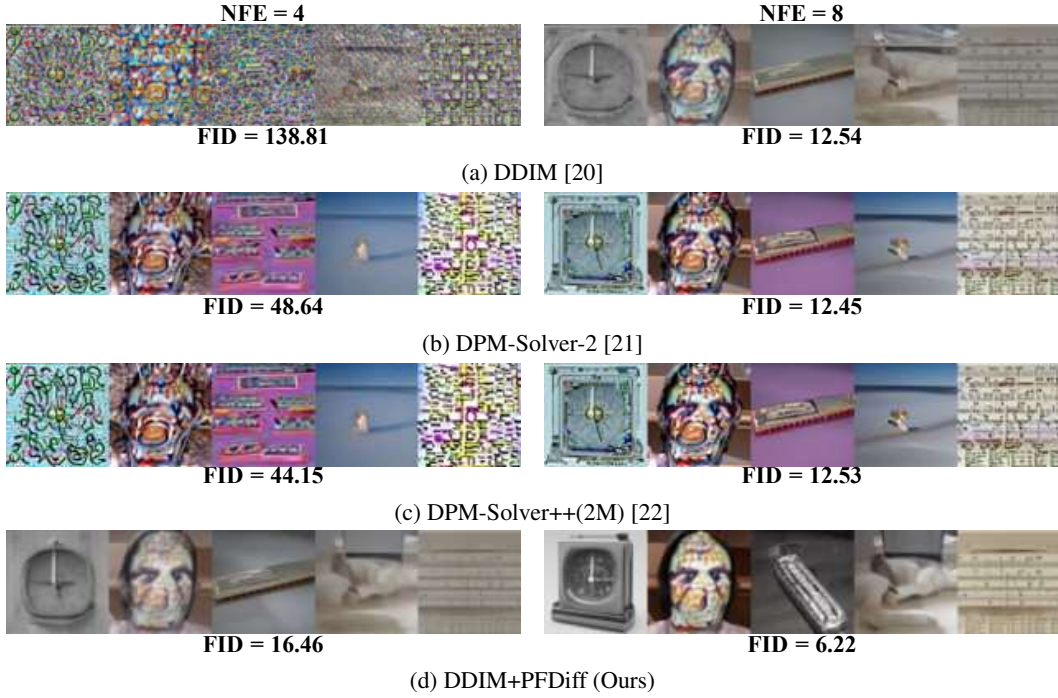


Figure 9: Random samples by DDIM [20], DPM-Solver-2 [21], DPM-Solver++(2M) [22], and PFDiff (baseline: DDIM) with 4 and 8 number of function evaluations (NFE), using the same random seed, uniform time steps, and pre-trained Guided-Diffusion [5] on ImageNet 64x64 [33] with a guidance scale of 1.0.

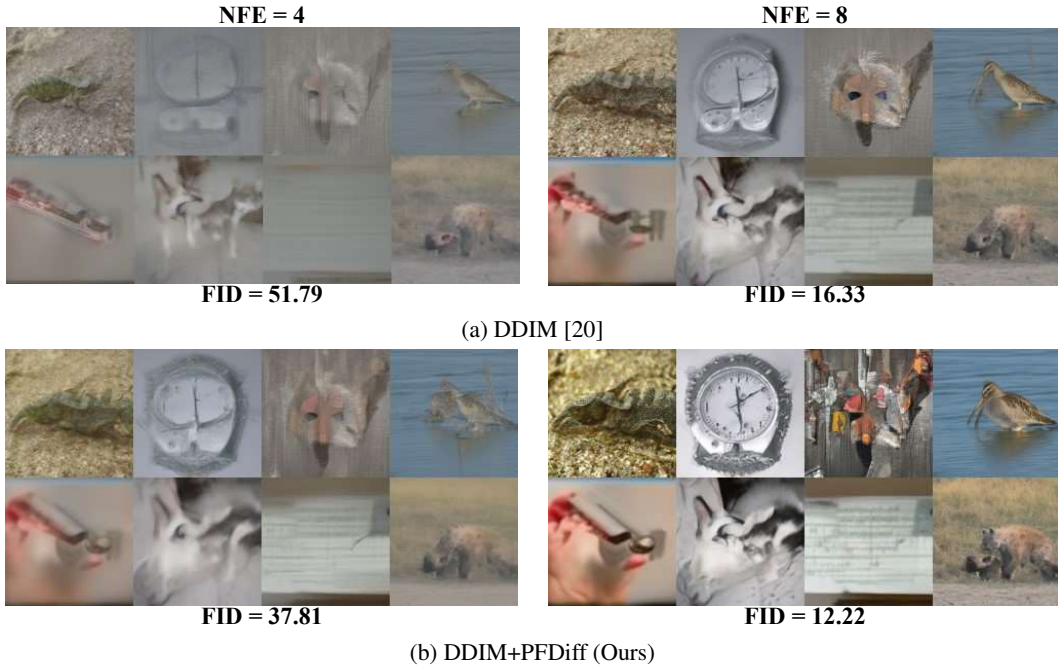


Figure 10: Random samples by DDIM [20] and PFDiff (baseline: DDIM) with 4 and 8 number of function evaluations (NFE), using the same random seed, uniform time steps, and pre-trained Guided-Diffusion [5] on ImageNet 256x256 [33] with a guidance scale of 2.0.

Text Prompts (listed from left to right):

A large bird is standing in the water by some rocks.

A candy covered cup cake sitting on top of a white plate.

People at a wine tasting with a table of wine bottles and glasses of red wine.

A bathtub sits on a tiled floor near a sink that has ornate mirrors over it while greenery grows on the other side of the tub.

A kitchen and dining area in a house with an open floor plan that looks out over the landscape from a large set of windows.

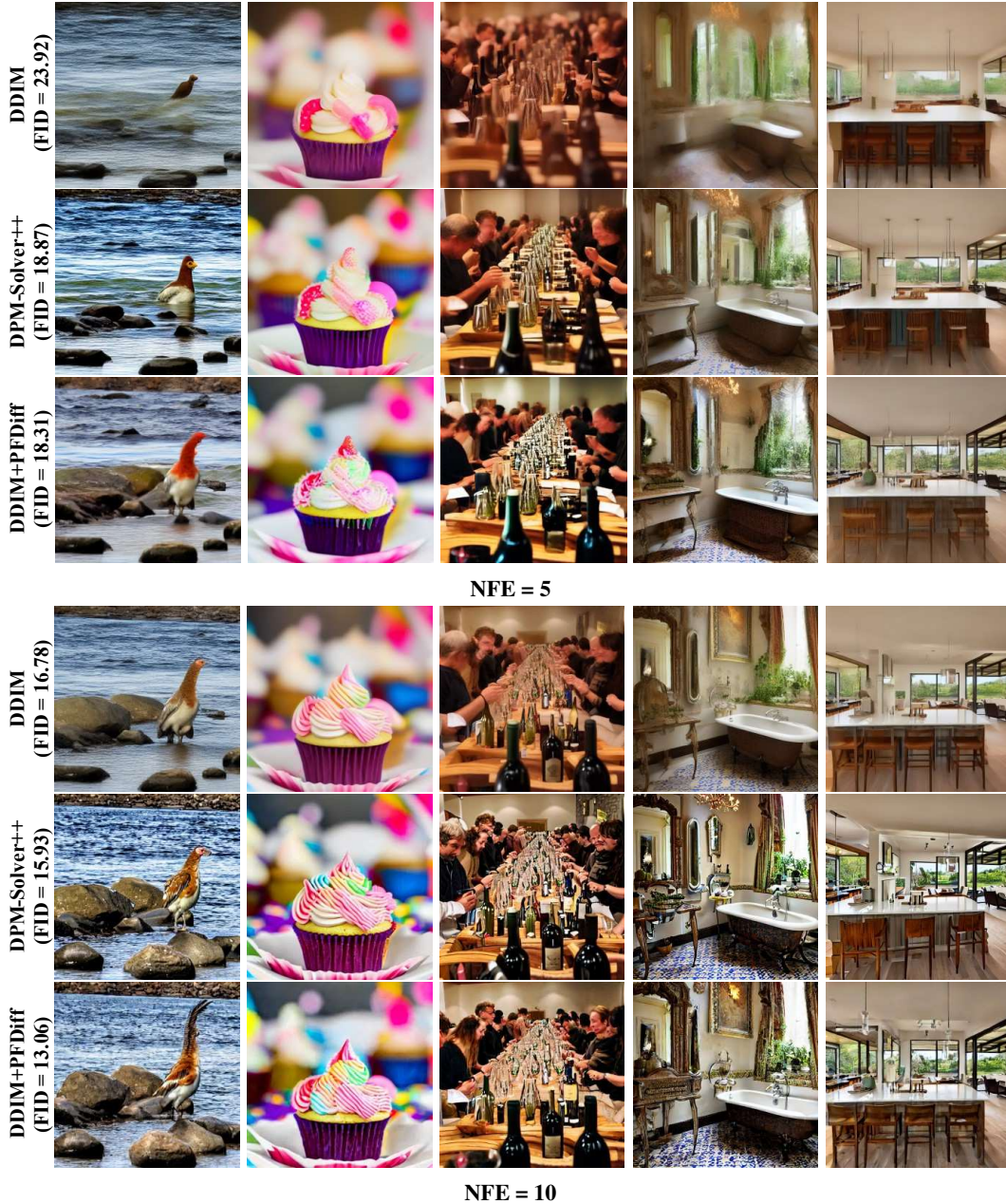


Figure 11: Random samples by DDIM [20], DPM-Solver++(2M) [22], and PFDiff (baseline: DDIM) with 5 and 10 number of function evaluations (NFE), using the same random seed, uniform time steps, and pre-trained Stable-Diffusion [9] with a guidance scale of 7.5. Text prompts are a random sample from the MS-COCO2014 [32] validation set.